MECHANICAL CHARATERIZATION OF A2 AND D2 TOOL STEELS BY NANOINDENTATION

Uzochukwu Chimezie Okafor

Thesis Prepared for Degree of

MASTER OF SCIENCE

UNIVERSITY OF NORTH TEXAS

May 2012

APPROVED:

Reza Mirshams, Committee Chair
Seifollah Nasrazadani, Committee Member
Cheng Yu, Committer Member
Enrighe Barbieri, Chair of Department of Engineering Technology
Costas Tsatsoulis, Dean of the College of Engineering
James D. Meernik, Acting Dean of the Toulouse Graduate School

Okafor, Uzochukwu Chimezie, Mechanical Characterization of A2 and D2 Tool Steels by Nanoindentation. Master of Science (Engineering Systems - Mechanical Systems), May 2012, 85 pp., 12 tables, 43 figures, references.

Nanoindentation technique was used to investigate the surface properties of A2 and D2 tool steel subjected to different heat treatments. The mechanical characteristics of these two easily available tool steels were studied based on microstructural images obtained from SEM, the grain growth after heat treatment using X-ray diffraction method and nanoindentation technique. The investigation showed that a single nanoindentation result can explain how heat treatment influences reliability and failure in A2 and D2 tool steels. In this work, the causes and effects of these variations were studied to explain how they influence reliability and failure in A2 and D2 tool steel. Finally, a cube-corner indenter tip was used to determine the fracture toughness of silicon wafer. The emphasis of this research is on how nanoindentation technique is more extensive in material characterization.

ACKNOWLEDGEMENTS

I want to thank my God for seeing me through this program successfully despite the all challenges along the way. My profound appreciation goes to my advisor Dr. Reza Mirshams for all his supports and encouragements all through this research work. At first, I was not sure of what to do and how to do it with regards to nanoindentation and material characterization but through his mentorship I was able to wade through the storms of countless lonely nights in the lab and ultimately believing in me to successfully conclude this research. I thank my committee members- Dr. Seifollah Nasrazadani and Dr. Cheng Yu, for their encouragements and insightful contributions, Dr. Leticia Anaya for her constant support, Dr. Hongbing Lu for allowing me to run some validations tests in his lab and his student Yingjie Du for staying with me in the lab for most nights. I would like to thank Ankit Srivastava for his technical support, patience and answers to all my queries with the Nanosuite software in the course of this research work. I will forever cherish the contributions you all made towards the fruition of my dream as this has helped me both professionally and personally.

This mission would not have been possible if not for the selfless sacrifices, prayers, and unweaving mental and financial support from my family and to them I would want to dedicate this master's work. M.s. Mercy Achu, Dr. Gladis Nwabah and family; I want to say thanks for been a there for me, you cushioned the absence of my immediate family for all these years. Not forgetting my friends Dayo, Iyke, James, Andrew, Dapo, also Chidi and Chukwudi. Most of all, my special thanks goes to Dr. Jumoke, Dr. Nonye, Ojite and Bede. You helped me not to cave-in in times of pressure. I would want to thank also all of those space can't allow me to list here who made my stay at the University of North Texas a wonderful experience and a nice journey.

TABLE OF CONTENTS

Page

LIST OF TABLES

Page

LIST OF ILLUSTRATIONS

Page

CHAPTER 1

INTRODUCTION

Reliability of engineering products and accuracy in probing their mechanical properties require a good understanding of the materials used in the manufacturing of the products. Occasionally, the use of conventional means to determine mechanical characters of engineering materials are inaccurate due to the errors built into the probing systems or due to human limitations on the side of the equipment operators. These often results in premature failure of machine parts or tools in active duty. This fact suggests that in order to ensure the high level of reliability needed in machine tool products, an in-depth knowledge of the properties which defines the distinctive behaviors of the material need to be accurately determined [1].

The concept of fracture has continued to evolve into a vast subject ever since its fundamental concepts were pioneered by Griffith, Irwin, Inglis and Orowan. Evidently, more fracture phenomena has emerged which has challenged researchers to develop more sophisticated tools as to provide further insight in areas of materials failure behavior. Fracture toughness is represented by the symbol K_{IC}, for which a lower value ofK_{IC}, indicates a greater chances of sudden failure due to pre-existing flaw [2]. It is noteworthy to point out that most engineering tools are used at or near design limits [2], conversely great care need to be applied in the selection of materials to be used for each particular design/ application. In order to establish this safe performance level desired in materials used in the manufacture of machine tools, the material's fracture toughness need to be determined. Fracture toughness in the most general of definitions is the ability of a material to withstand fracture in the presence of cracks [2]; this important design parameter has to be determined in order to select the right materials

and alloys suitable for the desired design specification. Usually, hardness in tool steels is increased by heat treatment but this method reduces toughness value. Therefore in order to optimize a materials' microstructure and its mechanical properties in design, desired material to be used for the application needs to be studied at a microstructural scale. Although there are various kinds of tests and equipment available for material characterizations, only few can be used to probe the mechanical properties of materials at a very small scale (Nano-10^{-9}). This renewed the interest on the importance of instrumented indentation testing (IIT) which has become increasingly important in different facets of science and technology for probing material's hardness, modulus of elasticity and other important mechanical properties [3-10].

Fig. 1.1. A Nanoindentation apparatus for nano-scale mechanical measurements (MTS Nano indenter XP®).

Nano indentation is a lower end range application of Instrumented Indentation Testing (IIT) and is based on standards for instrumented indentation testing by the American Society of Testing and Materials and International Standard Organization (ASTM E2546 and ISO 14577). Fig. 1.2 shows a simple diagram of the loading and unloading curve of a typical load-displacement test from a nanoindentation experiment.

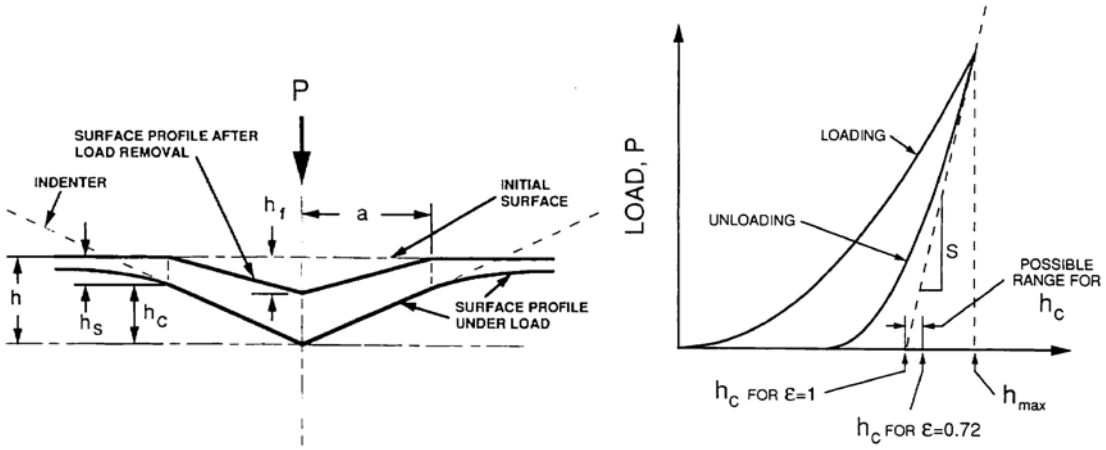

Fig. 1.2. Typical indentation load-displacement curve defining experimental quantities from loading to unloading point showing final and depth contact [32].

This is the idea behind the use of nanoindentation technique for material characterization, indentation test provides a more detailed and accurate means to measure mechanical properties of small material thereby eliminating human and machine errors which are common in conventional methods of material characterization.

The cube-corner indenter was used in this study because it substantially reduces the cracking threshold in the test of fracture toughness. A sharp indenter like the cube-corner tip which has an included angle of 35.26° between the axis of symmetry and a face, when used for fracture properties characterization, generates radical crack at fewer indentation loads than Vickers or Berkovich indenters. Vickers and Berkovich indenter has relatively large face angles of 65.27° and 68° respectively; using them for this test will likely cause deformation by expanding cavity model than slip-line theory thus generating a higher compressive force which is undesirable in fracture toughness test [9, 10]. In this study, nanoindentation technique is used to characterize fracture toughness K_{IC}, in tool steels materials (A2 and D2) heated to their respective austenitizing temperatures and then quenched (1) In open air, (2) In water mixed

with ice (10°C). The Indentation technique method used is based on the radial crack propagations which occur in brittle materials as shown in Fig. 1.2 when indented with a sharp tip [11].

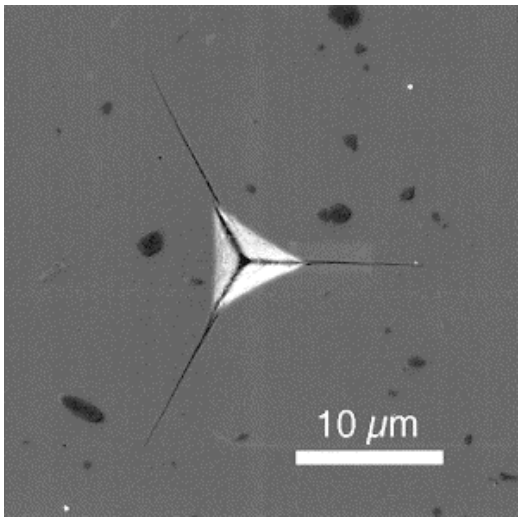

Fig. 1.3. Indentation on glass made with a cube-corner tip showing well defined radial cracks.

According to a previous work done by Lawn, Evans et al [12], fracture toughness, K_{IC}, and the lengths of the radial cracks, *c*, are related by a simple relationship of the form:

$$K_{IC} = \delta \left(\frac{E}{H}\right)^{1/2} \frac{P}{c^{3/2}} \quad (1)$$

where K_{IC} (MPa$\sqrt{m}$)is the fracture toughness, P (mN) is the peak load of indentation, δ is an empirical constant independent of the material and c (μm) is the length of the radial crack trace on the material surface after the indentation. E (GPa) and H (GPa) are properties which can be determined directly from the analyses of the nanoindentation load-displacement data. With an accurate means to measure the radial length, c, from the crack surface, the fracture toughness, K_{IC} for the examined material can be determined [11].

Heat treatment is important in the design of tool steels; a poorly conducted heat treatment will affect the quality of the end product and inversely affect its fracture toughness adversely.

A2 is an air or oil hardening chromium-molybdenum-vanadium alloyed material tool steel, normally regarded as the universal cold work steel. It has a very fine grain structure which gives it a superior-quality steel characteristic. It possesses deeper hardening ability, high compressive strength, good wear resistance, good hardenability and high stability after hardening. A2 tool steel is ideal for making thin parts that are normally prone to cracking during heat treatment.

D2 on the other hand is a versatile high-carbon/high-chromium tool steel that has gear wear and abrasion resistance. D2 offers high hardness and is commonly used for long-run dies and blanking as well as shear blades, burnishing tools and gages.

While A2 and D2 tool steel are known for their high wear resistance, and fracture toughness, the study of their material properties on a nano scale could mean possible reduction with minimal errors in their use in tool steel fabrication. This could also ensure improvement in their usage for machining activities which has seen tremendous growth in the early part of last century.

The purpose of this work:

- Study the effect of heat treatment on cutting tool materials
- Validate the hypothesis that shows the relationship between heat treatment, fracture toughness and carbon content of cutting tool materials

It is hypothesized in this study that since both D2 and A2 tool steel are of high carbon content, a rapid quenching after heat treatment of samples from both materials will increase their brittleness and subsequently make it easier to generate radial cracks on the tested surface through nano indentation.

CHAPTER 2

LITERATURE REVIEW

2.1 Fracture Mechanism and Modes

The catastrophic sinking of the passenger liner,*Titanic,* on her maiden voyage in 1912 causing the death of about 1500 passengers and crew members has been attributed to the brittle fracture of the steel superstructure. Research conducted on the retrieved hull by Dr. Robert Ballard and his team confirmed the hull was made of brittle steel material [64], the brittleness of the material is as a result of it high sulfur content and/or the high ductile-brittle transition temperature in the North Atlantic Ocean at that time.

In failures seen in materials, design or material flaw aggravated by a crack growth process causes crack to reach a critical size for eventual fracture. Some of the crack growth mechanism includes fatigue, stress-corrosion cracking, creep and hydrogen-induced cracking which can occur from cleavage, rupture or intergranular fracture. Crack can develop during service life from machining, quenching, fatigue or hydrogen embrittlement or during the design and fabrication stage of which brittle fracture is the most worrisome kind [41]. According to Griffith pioneering studies on fracture mechanisms, the discrepancy between theoretical cohesive strength and observed fracture strength could be explained by the presence of very small, microscopic flaws and cracks that always exists under normal conditions at the surface and within the interior of a material. Consequently, the energy involves in the fracture process / the fracture work done per unit area during fracture is given by:

$$\int_0^{\lambda/2} \sigma_c sin\frac{\pi x}{\lambda/2} dx = \sigma_c \frac{\lambda}{\pi} \qquad (2)$$

where σ = the tensile force necessary to pull atoms apart, σ_c = the cohesive strength, $\lambda/2$ = a sinusoidal force-displacement law with a half period. In Griffith's energy-balance criterion, a crack grows when the amount of energy released due to the increment of crack propagation is greater than the amount of energy been absorbed

$$\frac{dU}{da} \geq \frac{dW}{da}$$

where dU is the differential of the total energy released from the body due to the crack which is energy per unit area multiply by the volume:

$$U = \pi(2a)(a)B \frac{\sigma^2}{2E} = \frac{\pi\sigma^2 a^2 B}{E} \quad (3)$$

the volume of the material whose energy is released is assumed to be of an elliptical region around the crack as shown in Fig. 2.2 and dW represents the differential of surface absorbed energy

$$W = (2aB)(2\gamma_s) = 4aB\gamma_s \quad (4)$$

where $2aB$ is the area of the crack and $2\gamma_s$ is twice the surface energy per unit area to form two new fracture surfaces.

Further rearrangement after working out the derivatives in Eq. 2 produces the Griffith criterion for crack growth which is:

$$\sigma\sqrt{\pi a} = \sqrt{2E\gamma_s} \quad (5)$$

For the most part in the early 1940s fracture theory was based on the critical strain energy release rate, G_o, required for crack growth was equal to twice an effective surface energy, γ_{eff}.

$$Gc = 2\,\gamma_{eff} \quad (6)$$

where γ_{eff} represents the plastic energy absorption around the tip of the crack, and a fraction

attributed to the surface energy of the crack surface. In recent times, the stress field around the crack the surface energy has been supplemented by the stress-intensity factor, K, and a critical value of K for crack growth, K_c. Note that K_c is the critical value for which crack grows when it is exceeded by a combination of applied stress and crack length. K_c is also known as plane-strain fracture toughness, K_{IC} . This is the foundation of the relationship between flaw size and fracture stress which can be lower than yield strength depending on crack length and geometry.

2.2 Defects in Solids

The presence of irreversible damages in material causes them to possess low fracture strength relative to their theoretical capacity; as such they deform plastically at much lower stress levels. Sometimes, defect in materials could be as a result of a faulty manufacturing process or microstructural in origin. These defects include quench cracks, porosity and shrinkage cavities grinding or microstructural in nature, such as inclusions, brittle second-phase particles and grain-boundary films which can lead to crack formation if the stress level exceeds the critical level, K_c, as explained above.

In search of weak points in material, note that crystal (pure) material contains no alloying constituents whereas materials use for structural designs contain alloys materials to strengthen their characteristics. Also, large parts of a component technically have higher tendency for premature failure than small parts because the larger part contains more faults/defects than the smaller ones. In classifications of material failure modes, the crystal structure of the material is of high importance because it determines how the material competes between flow and fracture. Fracture in engineering materials either along the grain

boundaries (intergraunal) or through the grain (transgranual) occurs mainly through four kinds of fracture modes:

- Ductile fracture from microvoid coalescence
- Fatigue
- Brittle fracture from cleavage, intergranular fracture and crazing
- Decohesive rupture

Table 2.1: Material properties and their effect on fracture behavior.

Physical property	Increasing tendency for brittle fracture
Electron bond	Metallic $\rightarrow$Ionic $\rightarrow$Covalent
Crystal structure	Close-packed crystals $\rightarrow$Low-symmetry crystals
Degree of order	Random solid $\rightarrow$Short-range order $\rightarrow$Long-range order solution

2.3 Ductile Fracture from Microvoid Coalescence

The presence of particles or micropores in ductile matrix of engineering materials, mostly metallic alloys act as fracture initiators due to decohesion between the particle interface, fracture of the particle or even the combination of the two.

These microvoids are not same as micropores possessed in a material as a result of casting or powder sintering procedures. The nucleation of these microvoids could be complex and depends on a lot factors including inclusion size, stress and strain levels, local deformation modes and alloy purity [42]. The mechanical properties of the particles, the properties of the matrix interface, the size and the distribution of the particles and the plastic properties of the

matrix are factors that affect the fracture toughness of materials that fail by microvoid coalescence.

2.4 Brittle Fracture from Cleavage

Fracture in brittle materials is commonly known as cleavage fracture. It occurs by direct breaking of atomic bonds along the specific crystallographic planes. Cleavage usually involves a low-energy fracture and the surface of the fractures is flat, bright and shiny. Cleavage fracture is mainly seen in BCC, HCP, and ionic and covalently bonded crystals, also in FCC metals that are subjected adverse environment conditions. The “flow “of the “river pattern” seen in cleavage step is believed to be the direction of microscopic crack propagation because the fracture mechanism spreads through grain and grain boundaries. The likelihood of brittleness grows in some material grows at low temperature, higher loading rate and exposure to sever environment.

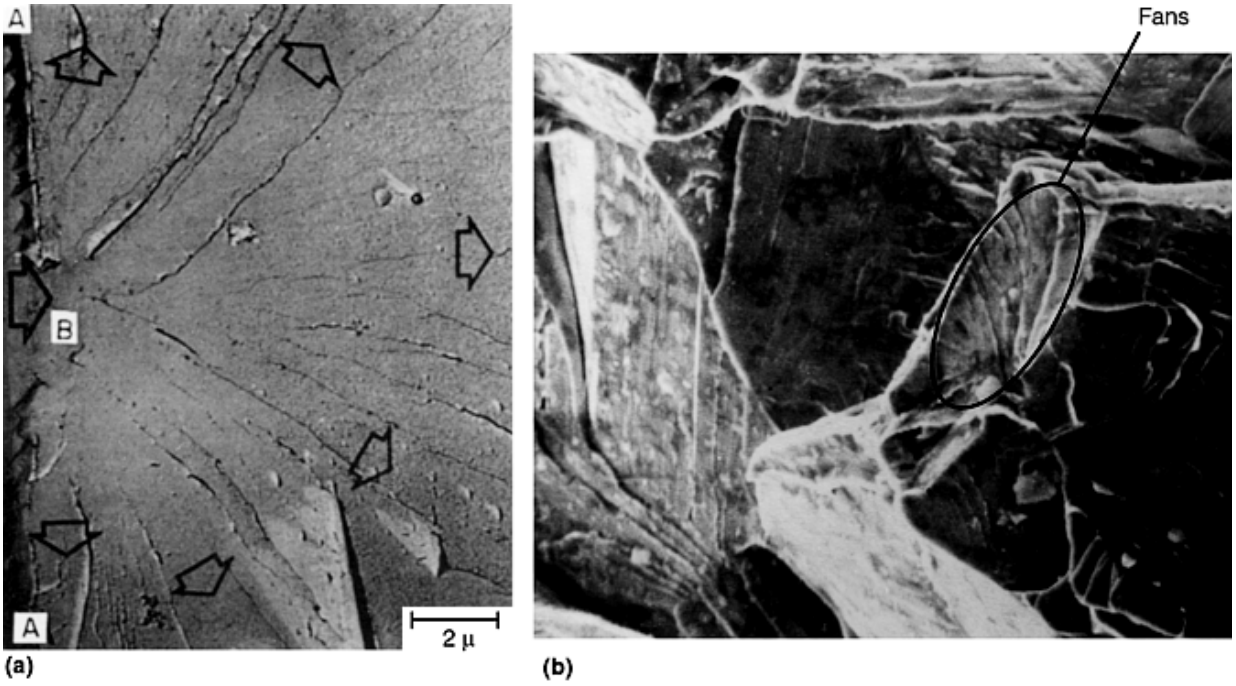

Fig. 2.1. Cleavage fracture [67, 68].

2.5 Fatigue Fracture

Under unsteady and cyclic stress fatigue failure can occur at a considerably lower than tensile or yield strengths of the material. Fatigue accounts for about 90% of bridge, aircraft and machine components failures. This form of failure is brittle-like even in a normal ductile material that is why it is sudden and catastrophic. The process of fatigue fracture involves crack initiation, crack propagation and final fracture. All these are dependent on the stress conditions, specimen geometry, the size of flaw in the material and the materials mechanical properties**.** The initiation stage usually extends over a small percentage of the fracture surface but may require many loading cycles if the nucleation process is slow. The orientation of a Stage I crack shifts to permit the crack to propagate in a direction normal to the loading direction [42]. The plane-strain condition determines the plane on which the Stage II crack propagates relative to the stress state.

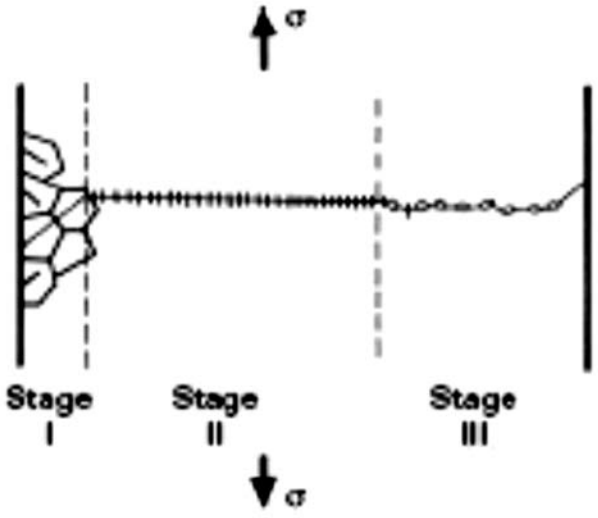

Fig. 2.2. Stages I, II and III of fatigue crack propagation [66].

The first stage involves the accumulation of dislocations on the surface near stress concentrations and form structures called persistent slip bands after a number of loading cycles. The area that rises above is extrusion and the area that falls below is intrusion of the surface which is due to the movement of material along the slip planes. This movement of material along the slip planes leaves tiny whole on the surface that serves are stress risers where tiny cracks can initiate along planes of high shear stress which is often 45° to the loading direction. Fatigue crack may start out at 90° to the plate surface but complete its propagation at 45° to the surface and sometimes could propagate immediately at 45° if the plastic zone size to plate thickness ratio were high enough, reflecting plane-stress conditions [42].

2.6 Boundary Decohesion

Boundary decohesion, sometimes referred to intergranular fracture and particle matrix debonding is an important mode of fracture. It occurs when the boundary is the weak link in the microstructure.

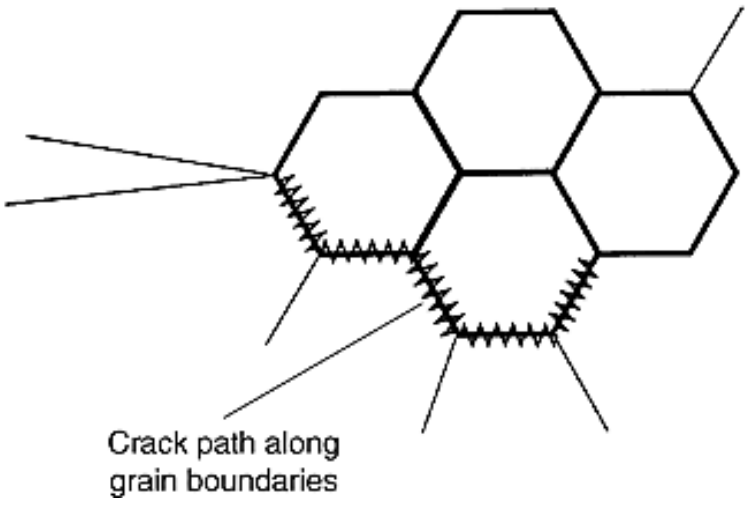

Fig. 2.3. Intergranular and particle matrix debonding [65].

Particle debonding significantly changes the magnitude and location of plastic slip in vicinity of the particle. Some conditions existed for this to occur:

- There is no deformation of the grain interiors; however the boundary strength is lower than the cleavage strength
- Weakening has occurred at the boundary due to segregation of the damaging species
- The nucleation of brittle particles on the boundaries which acts as crack initiators providing an easy path for fracture whereas the boundary remains strong
- Adverse environmental impact on the strong boundary. This condition is time dependent as the damaging species must diffuse into the material ahead the crack tip

Heat treatment and chemistry affects the distribution of boundary particles. Heat treatment can increase a material's boundary particle toughness and thus reduce its chances of boundary decohesion.

2.7 Fracture in Tool Steels

Tool steels are special materials designed to function and perform different task in accordance to design specifications. However, in even in the most controlled environment and sets of operation control, is each type of tool steel has its operational limits. These limitations which could preexist in the material or arise during the service year of the tool can cause the shortening the tool life and in some case cause a catastrophic failure. In the selection of materials and factors for high performance of tool steels the following need to be considered:

- Good mechanical design
- Proper selection and application of alloy

- Proper finishing by grinding and EDM
- Correct heat treatment
- High-quality steel

In tool steels, there are major causes of premature failures namely: (1) the source of stress and (2) the condition of the microstructure. Poor mechanical design can cause excessive stress to be concentrated on part giving rise to premature failure notwithstanding the standard manufacture process. Conversely, the presence of flaws can lead to a premature failure of part even though the design was properly done.

The ability to withstand fracture, possess high strength and resist wear is very desirable in tool steels. Fracture in tool steels could be stress controlled or strain controlled, in the former fracture is largely cause by stress without any applicable plastic flow and in the latter, plastic deformation precedes fracture. The topic of fracture has been approached in different ways, it can be grouped as intergranular or transgranular, brittle or fracture. Fracture on the other hand can be grouped on the basis of environmental effects and embrittlement mechanism. Brittle fracture is a strain-controlled fracture that occurs through the mechanism known as microvoid coalescence. There are some characteristics of ductile fracture:

- Plastic deformation precedes the fracture
- Fracture termination areas have shear lips
- Fibrous nature of the fracture surface
- Crack growth is slow

Microvoid coalescence and transgranular fracture are seen in ductile fracture from a microscope point of view. The nucleation site for ductile fracture can be the interface between

two ductile phases, however microvoids can form interfaces between the matrix phase and inclusion. In pure metals of low-strength, fracture could occur without any evidence of microvoid. The surface of ductile fracture tends to be macroscopically flat, smooth with silky appearance and consistent of fine microstructure of properly processed tool steels.

2.8 Brittle Fracture

Stress-controlled failure is seen in brittle fracture that occur with little or no-plastic deformation. These stresses are well below the materials ultimate tensile strengths or reasonable operating conditions. Metals of body-centered cubic (bcc) and hexagonal close-packed (hcp) orientation can experience brittle fracture but not face-centered body (fcc) metals expect in special cases. Factors that can influences brittle fracture include strain rate, stress rate, composition, microstructure, grain size and specimen size. The presence of cleavage cracks which propagates into the matrix structure of the material can act as an initiation point for brittle fracture. Intergranular cracking along the embrittled austenite grain boundaries is a major mechanism of brittle fracture in tool steels and high carbon steel. The presence of hydrogen increases the initiation of this form of brittle fracture which is caused by austenitizing. The size of the grain influences the initiation and propagation of brittle fracture as shown in Hall-Petch equation:

$$\sigma_c = \sigma_0 + kd^{1/2} \quad (7)$$

where σ_c is the cleavage strength, d is the grain diameter, and σ_0 and k are constants. Interagranular fracture is promoted by coarse austenite grain size, phosphorus segregation to precipitation on grain boundaries which arises due to tensile stresses or bending stresses

generated by heat treatment or in service [44]. Chevron fracture pattern is frequently observed in low-strength steels, patterns are as a result of discontinuous growth pattern. Studies show that the chevron pattern is caused by a combination of discontinuous regions of cleavage fracture joined by regions of shear; the chevron features are the ridges between the cleavages and shear zones [45].

Some remarkable features of brittle fracture include:

- There is no little or no plastic deformation before fracture
- Fracture surface is usually flat and perpendicular to the surface of the component
- The growth of the crack is rapid

2.9 Fracture Toughness

The measure of a material's (ceramics or brittle) resistance to fracture is extensively determined with fracture toughness (K_{Ic}) values [47]. Fracture toughness, K_{Ic}, is dependent on the condition of the operation which includes environment or the loading rate. The toughness of a material can be defined as the amount of energy that is absorbed the crack is advanced one unit of area. The unit is force x length/length^2. There are different kinds of test technique that could be used to determine fracture toughness in engineering brittle material [47] though there is no specific standard specimen. The technique to use at any prevailing situation is based on the kind of information that is wanted which is based on the localized fracture energy around the flaws. A comprehensive approach to determine fracture toughness will consider the specimen geometry, preparation and fabrication history in correlating test specimen behavior to actual component fracture toughness.

2.10 Conventional Techniques to Determine Fracture Toughness

Chevron notch method: This use of small sizes of material makes this methods' acceptance high. The loading geometry, highest value of load and the specimen, all counts for the proper calculation of fracture toughness in a material. The method required no material constant but a complex specimen space is required which is an extra machining cost. It consists of a notch introduced in a test bar which is of about 3 x 4 x 50mm, with varying angle of 30° to 50°. The bar or rod is precracked at a crosshair slow rate of 0.005mm/min and then loaded to failure at a rate of 0.05mm/min based on a two-step technique which has produced more accurate results than the single loading approach [48]. The crack at the tip of the chevron propagates stably as the applied force is increased until it suddenly fractures. Fig. 2.9 shows a plot of load versus crosshead motion.

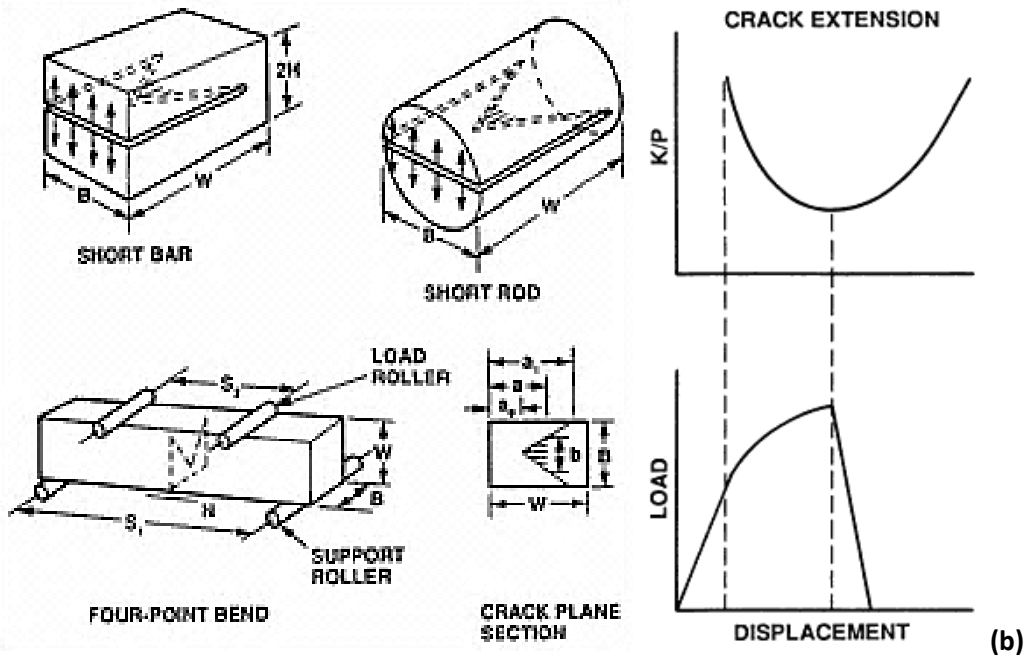

Fig. 2.4. (a) Bar and rod configuration of chevron notch test (b) Load-displacement correlation showing maximum load at for fracture toughness computations [69].

Double-cantilever beam method: In this method, any of the three different loading configurations (wedge load, applied load or applied moment) can be used. The fracture toughness is derived from the notched length, specimen dimensions, and normal tensile load. Freiman et al [49] did a pioneer work on this method in other to eliminate the need for a tapered specimen section. The importance of these methods over other fracture toughness measurement method includes:

- The independence of stress intensity from crack length in the case of the constant applied moment loading
- The simple nature of sample preparation and the testing procedures

The specimen is precracked in order that the crack propagates (failure) from the shape flaw of the right geometry. If this is not done, the crack normally grows away from the tip of the notch and usually produces anomalously higher fracture toughness value.

Single-edge precracked beam**:** Nunomura and Jitsukawa applied this technique to create and arrest a brittle crack in bearing steel [50]. The method involves loading fixture of precracked beam-shaped specimen compressively against a centrally located groove in an avail. A straight-through crack line is created from an indentation crack. The straight line is created by applying a load (bending) on a specimen of precracked fixture. The test sequences are:

(1) Stable growth of the initial precracked indentation crack

(2) Detection of pop-in

(3) The arrest of the median crack as a straight line through the thickness of the specimen

Steel toughness values varies base on the kind of heat-treatment used to strengthen it

and the different densities of carbides dispersions. Different testing technique affects and nature of the test affects the toughness value of steel.

Fracture toughness values can be obtained through different means and as such the results can't be compared directly. In other to obtain a standard result, care must be given to the testing procedures in other to minimize error from the machine or the operator, sample preparation, and the material composition both microstructural or heat treatment processes. The presence of alloying and heat treatment can affect the values of toughness in material. Lower carbon content, which lowers strain-hardening rates of the tempered matrix martensite, and lower alloy content, which reduces the volume fraction of hard alloy carbide particles that initiate fracture, is used to increase the fracture toughness at the expense of wear resistance.

Table 2.2: Effects of alloying elements on steel.

Aluminum	Deoxidizes and restricts grain growth
Boron	Increases hardenability
Carbon	Increases hardenability and strength
Chromium	Increases corrosion resistance, hardenability and wear resistance
Lead	Increases machinability
Manganese	Increases hardenability and counteracts brittleness from sulfur
Molybdenum	Deepens hardening, raises creep strength and hot-hardness, enhances corrosion resistance and increases wear resistance.
Nickel	Increases strength and toughness
Phosphorus	Increases strength, machinability, and corrosion resistance
Silicon	Deoxidizes, helps electrical and magnetic properties, improves hardness and oxidation resistance
Titanium	Forms carbides, reduces hardness in stainless steels
Tungsten	Increases wear resistance and raises hot strength and hot-hardness
Vanadium	Increases hardenability

2.11 Nanoindentation

The concept of indentation tests had its root in Mohr's hardness test of 1822 in which materials were categorized base on their ability to leave permanent dent on another materials. They were ranked on a scale of 1 - 10 with diamond assigned the highest point of 10 on the scale [10]. Consequently, with constant improvements on this old concept, indentation technique has evolved into present day state-of-the-art indenters use in different fields of science. The study of materials on nano scale (one billionth, 10^{-9}) underscores the conscious and continual exodus from the traditional means of research and development to a most accurate but sophisticated continuum in a quest to find answer to theories that defines material behaviors/properties which revolve around atomic scale.

With the present advert of microelectronics and micro-electro-mechanical systems (MEMS); it is observed that as a specimen's physical dimension approaches microstructural scale, its mechanical properties begins to exhibit a dependence on the specimen size. In metallic thin film, this change causes yielding to occur in way as opposed to their bulk counterparts. This phenomenon has been observed, but no in-depth understanding of it was arrived on then [14]. In his famous lecture "There's Plenty of Room at the Bottom," physicist Richard Feynman at an American Physical Society meeting at the California Institute of Technology (CalTech) on December 29 1959, described a process in which scientists would be able to manipulate and control individual atoms and molecules. However, it was until the 1980s invention of the scanning tunneling microscope (STM) that the manipulation of atoms and molecules were possible which has resulted to significant changes in the field of science.

Nanotechnology is currently undergoing various developmental improvements which are akin to the early commercial application of information technology in the late 1960s [15]; more impressive discoveries that will lead to great transformation in the technological world are still anticipated.

To carry out experiment at the nanoscale (10^{-9}) rather than in microns (10^{-6}) or millimeters (10^{-3}) has many distinguishing advantages like, the ability to measure indirectly the contact area at full load which couldn't have been done through conventional means. Bousessinesq [16] and Hertz [17] in their research developed a method base on theory for computing the stresses and displacements in an elastic body loaded by a rigid axisymmetric indenter in view to address the elastic contact problems which are vital in the analysis procedure, the latter analyzed the problem of elastic contact between two spherical surface of different radii and elastic constants and came up with tremendous great results that aids research work in field mechanics. Sneddon [20, 21] in his work derived a general relationship among the load, displacement and contact area for any punch that can be described as a solid of revolution of a smooth function. The load-displacement relationships from his result could be written as: $P = \alpha h^m$

where P represents the indenter load, h is the elastic displacement of the indenter and α and m are constants and its values for some punch geometries includes m=1 for flat cylinders, m=2 for cones, m=1.5 for sphere in the limit of small displacements and m = 1.5 for paraboloids of revolution.

According to Oliver and Pharr [30], the modeling of indentation contact so that it includes plasticity is complex and analytical solutions are hard to obtain [22], thus finite

element method and experiments were used in other to have a better understanding of the importance of plasticity in indenter contact problems.

Tabor [55] and Stillwell [56] in their studies of mechanical properties of metal using load-displacement sensing indentation method with conical indenter noticed a unique shape of the hardness impression after the indenter is unloaded and the material elastically recovers. A spherical shape was obtained when spherical indenter was used and a conical shape was obtained when a conical shape was used. This experiment offered a lot of importance in depth sensing technique because it shows the elastic solution that exist for individual indenter geometry, therefore the ways in which plasticity affects the interpretation of elastic unloading data can be dealt with by taking into account the shape of the perturbed surface in the elastic analysis. Tabor showed from his results that the shape of the unloading curve and the amount of recovered displacement for the conical and spherical indenter can be accurately calculated in relation to the elastic modulus and the size of the contact impression. Bulychev, Alekhin, Shorshorov and co-workers [16-17, 23, 24, 26, 31] in their work in 1970s saw the potential on how to use the load-displacement sensing indentation testing as way to extract elastic modulus and hardness.

Thus, instruments for measuring submicron indentation was developed in the 1980s when it was realized that the load and depth sensing indentation methods could be useful to in measuring mechanical properties of thin films and surface layers [29]. A more comprehensive method for determining modulus from indentation load-displacement data was put together by Doerner and Nix [25] by observing the unloading stages, the elastic behavior of the indentation contact similar to a flat cylindrical punch; in other words as the indenter unloads the contact

area remains constant. Doerner and Nix suggested that the unloading stiffness can be computed from a linear fit of the upper one-third of the unloading curve however, rarely has it been observed that unloading curve is linear even in the initial stage of unloading.

The only part that is recovered during the withdrawal is the elastic portion of the displacement. At the contact area,h_c, the project contact area of the hardness impression, A, is estimated by evaluation of the indenter shape function which is $A=f(h_c)$.

The cross-sectional area of the indenter to the distance,d, from the tip corresponds to the shape function $f(d)$.

Fixing the unloading curve to the power-law relation which is an elaboration of equation (2) according to Oliver-Pharr [30] we have;

$$P = B\left(h - h_f\right)^m \qquad (8)$$

where P is the indentation load, h is the displacement, B and m are empirically determined fitting parameters and h_f is represents the final displacement when unloading is completed. The most commonly determined mechanical properties; Young modulus and hardness, of many materials can be measured using these methods with great accuracy of about 10% [18] once a good experimental skill and careful analysis are in employed. The effects of pile-up can lead to over estimation of E and H in some materials where pile-up can occur around the hardness impression. Sink-in or pile-up can occur depending on the mechanical properties of the material in the case of elastic-plastic contact.

2.12 Olivier and Pharr Improved Technique

Around early 1970s, Bulychev, Alehin, Shorshorov et al recognized that there is a

possibility to measure elastic modulus and hardness from a single simple test [26, 31] in which the important quantities from the test are the peak load,P_{max}, the displacement at peak load,h_{max}, and the initial unloading contact stiffness, $S = dP/dh$, which is the slope of the initial portion of the unloading curve. The unloading data of the plot are analyzed according to a model for the deformation of an elastic half space by an elastic punch which relates the contact area to peak load to the elastic modulus [32]. It was on this premise that Olivier and Pharr generated the basic technique to calculate hardness and modulus of elasticity. Hardness from nanoindentation point of view is defined as indentation load divided by projected contact area which is the mean pressure the material will support while the elastic modulus is from the initial unloading contact stiffness.

$$H = \frac{P_{max}}{A} \tag{9}$$

$$S = \frac{dP}{dh} = \frac{2}{\sqrt{\pi}} E_r \sqrt{A} \tag{10}$$

where E_r is the reduced modulus and A is the projected area between the indenter and the sample, a quantity that is determined through area function, $A(h)$, is obtained from calibration indents performed on fused quartz sample. The accuracy with which nanoindentation property measurements can be made is integrally tied to how well Eq. (10) models real material behavior [33]. Also, the reduced modulus, E_r accounts for the effect of the non-rigid indenters on the load-displacement behavior through the equation

$$\frac{1}{E_r} = \frac{(1-v^2)}{E} + \frac{(1-V_i^2)}{E_i} \tag{11}$$

where E and v are Young's modulus and Poisson's ratio for the specimen and E_i and v_i are the Young's modulus and Poisson's ratio for the indenter. With knowledge of the material

properties of the diamond indenter ($E = 1140$ Gpa and $v = 0.07$), the modulus of indentation for the sample may be calculated:$E_{ind} = (1 - v^2)/E$. The elastic modulus can be determined from the indentation experiment if the Poisson's ration is known.

Over the years, nanoindentation technique has gone through a series of improvements for the purpose of investigating mechanical properties of materials on the submicron scale. Consequently, a correction factor has been added to the Sneddon's equation for accuracy in measuring mechanical properties.

$$S = \frac{dP}{dh} = \beta \frac{2}{\sqrt{\pi}} E_r \sqrt{A} \qquad (11)$$

β in the above equation is a constant that depends of the indenter geometry and is different for different kinds of indenters.

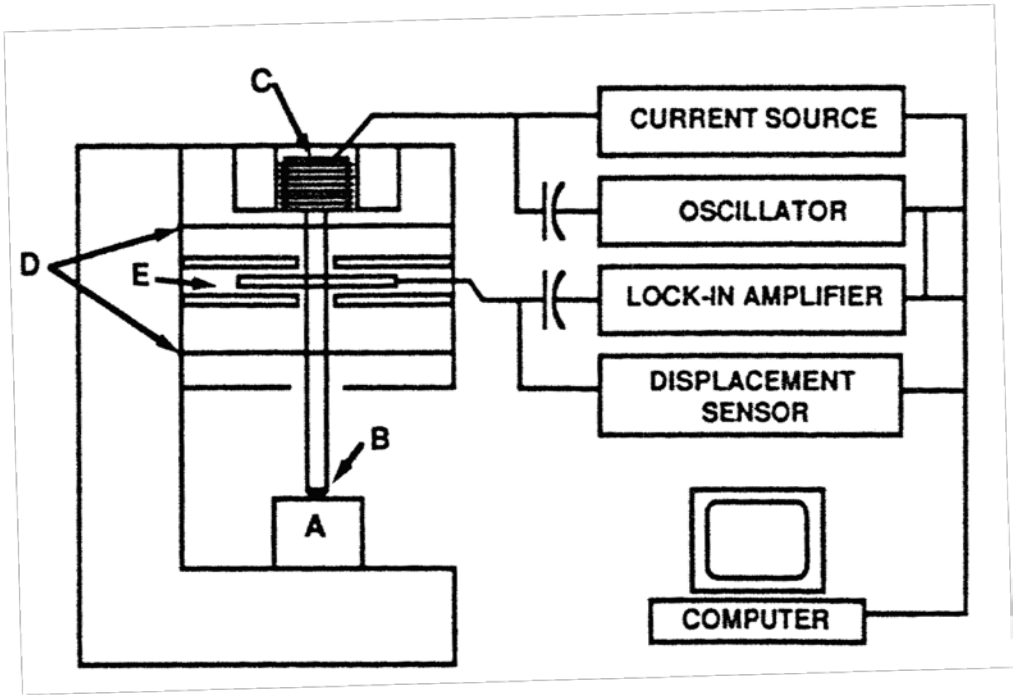

Fig. 2.5 Schematic representation of a nano indenter showing (A) the sample; (B) the indenter; (C) load application coil; (D) indentation column guide springs; (E) capacitive displacement sensor [32].

The indenter shape function are then used to independently estimate the contact area and separate measurements of E and$H$. The modulus can derived by measuring the initial unloading stiffness and with the contact area assumed to be equal to the optically measured area of the hardness impression. According to Oliver, Pharr and Brotzen [27], equation (9) applies to any indenter that can be described as a body of revolution of a smooth function. The derivations from equation (9) for flat ended punches with square and triangular cross sections are only 1.2% and 3.4% respectively as confirmed by the finite element calculations by King [28].

2.13 Area Function

Although the ideal area function sometimes provides the accurate description of the contact geometry at larger contact depths, deviations from geometrical perfection near the indenter tip, must be properly taken into account when measurement are to be made at small scales. Independent methods are used to determine the area function of tips. This is important because in pyramid indenters there could be variations from the ideal self-similar geometry which is caused by tip blunting, also the result produced can be inaccurate. The area function of an indenter tip is made by making a series of indentation at various depths in a Fused Silica. This can also be done using the dynamic stiffness measurement, with the benefit of obtaining the required data in a few tests. Since the elastic modulus of a material is independent of depth base on basic assumption, it is important to choose materials that contain no oxides or contaminants that will alter the near-surface elastic properties. Pile-up is greatly discouraged

since its influence is not accounted for in the procedure on contact depth. Area function calibration is implemented by making series of indents at a depth over an area of interest.

The plot of A versus hc gives the graphical representation of the area function, the curve can be fitted using any of the number of functional forms.

$$A = C1d^2 + C2d + C3d^{\frac{1}{2}} + C4d^{\frac{1}{4}} + C5d^{\frac{1}{8}} + \cdots \quad (12)$$

where the first term in the expression represents the ideal area function of an indenter (pyramid or conical) on condition that $C1 = F1$.

2.14 Geometry of Different Types of Indenter

Nanoindentation test are generally made with either spherical or pyramidal indenters. Standard nano indenters have to within the ranges specified by the ISO 14577-2 (Instrumented indentation test for hardness and material parameters, part 2: Verification and calibration of testing machines) which defines internationally accepted micro and nano indenter tolerances. Fig. 2.6 shows an indenter with its three parts, the diamond, the holder and the bond. The shaper the tip, the shallower an indenter can be made to give reliable hardness values. For an ideally plastic indentation, $h_c \approx h_t$, and for an elastic/plastic indentation, $h_c < h_t$. The ideal tip function for the ideal Berkovich tip is, $A = 24.56h_c^2$, experimental tip function for a Berkovich tip is given as $A = 24.26h_c^2 + \sum_{i=0}^{7} C_i h_c^{\frac{1}{2^i}}$

The accuracy and repeatability of calculated properties depend directly on the quality of the fundamental force and displacement data. All the forces used for indentation test are imposed on the indenter shaft by passing current through a coil that sits within an annular

magnet. Material that contains diamond or diamond particles will damage the indenter, the things that may affect modulus/hardness and stiffness results are:

- Surface roughness
- Surface flatness
- Material porosity
- Creep and homogeneity of surface.

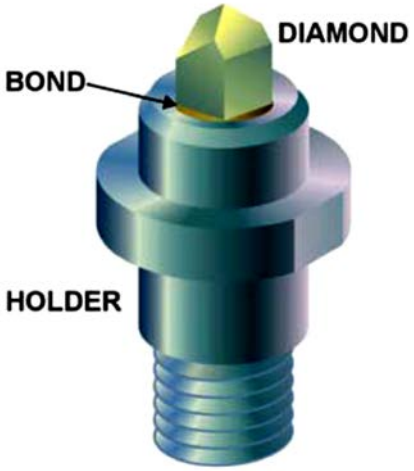

Fig. 2.6. A nanoindenter tip [71]

Different kinds of indenter shape are available such as three sided pyramids, four sided pyramids, wedges, cones, cylinders and sphere which can have sharp, flat, or rounded, a cylindrical or spherical shape. Materials like diamond, sapphire, quartz, tungsten, steel and tungsten carbide can be used for manufacturing them. The nano indenters are mounted on holders as designed by the manufacturers of the nano indenter equipment.

2.14.1 Berkovich Indenters

The most frequently used indenter in material characterization is the Berkovich indenter, it has a large includes angle of 142.3° which minimizes the influence of friction. The Berkovich indenter is designed to have the same area as the four-sided Vickers indenter at any given indentation depth, however the Berkovich geometry is preferred to the Vickers because a three-sided pyramid can be ground to a point thereby maintaining its self-similar geometry to very small scales. Some of the advantages of a Berkovich indenter include:

- Ideal for most testing purposes
- Readily manufactured
- Can induce plasticity at very small load, a good property in the measure of hardness

The Berkovich indenter tip is recommended for the following testing applications:

- Bulk materials
- Thin films
- Polymers
- Scratch testing
- Wear resistance
- Micro-electromechanical systems (MEMS)

Projected area for a Berkovich tip is given as

$$A_{proj} = 3\sqrt{3}h_c^2 tan^2\theta$$

$$A_{proj} = 24.56h_c^2 \text{ where } \theta = 65.3^0$$

2.14.2 Cube-Corner Indenter

The cube-corner indenter is another types of three sided pyramid with mutually perpendicular faces arranged in a geometry like the corner of a cube. The centerline-to-face angle for this indenter is 34.3°, whereas for the Berkovich indenter it is 65.3°. The sharpness of the cube corner produces much higher stresses and strains in the area of contact which makes it suitable to be used in the estimation of fracture toughness in brittle materials. The cube-corner tip is useful in producing very small, well-defined cracks around hardness impressions. The cube-corner indenter tip is recommended for the following applications:

- Thin films
- Scratch testing
- Fracture toughness
- Wear testing
- MEMS
- In-situ imaging

The projected area for a cube-corner indenter tip is given as

$$A_{proj} = 3\sqrt{3}h_c^2 tan^2\theta$$

$$A_{proj} = 2.5787h_c^2 \text{ where } \theta = 35.56^0$$

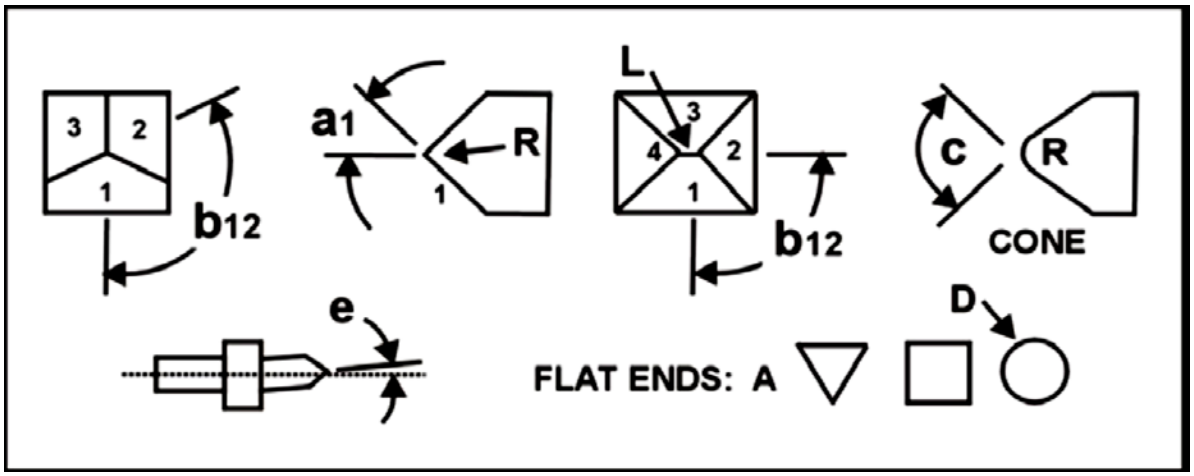

Fig. 2.7. Cube-corner indenter tip

2.14.3 Conical Indenter

A final indenter worth of mentioning in this work is the cone indenter. It has a sharp, self-similar geometry, but the simplicity of its cylindrical symmetry makes it attractive from a modeling standpoint. In fact, many modeling efforts used to support IIT are based on conical indentation contact. The conical indenter is attractive because the complications associated with the stress concentrations at the sharp edges of the indenter are absent. This tip has not always been used in most IIT testing because it is difficult to manufacture conical diamonds with sharp tips, this makes them of little use in the small-scale work around which most of IIT has developed. The projected area for a conical indenter tip is given as:

$A_{proj} = \pi h_c^2 \ tan^2\theta$

$A_{proj} = 9.42 h_c^2$ where $\theta = 60^0$

Table 2.3: Indenter tip and geometry.

Indenter type	Projected area	Semi angle θ (deg)	Effective cone angle α (deg)	Intercept factor∗ ε	Geometry correction factor β
Sphere	$A = \pi 2Rh_p$	N/A	N/A	0.75	1
Berkovich	$A = 3\sqrt{3}h_p^2\, tan^2\theta$	65.27°	70.3°	0.75	1.034
Knoop	$A = 2h_p^2 \tan\theta_1 \tan\theta_2$	$\theta_1 = 86.25^\circ$, $\theta_2 = 65^\circ$			
Cube-Corner	$A = 3\sqrt{3}h_p^2 tan^2\theta$	35.26°	42.28°	0.75	1.034
Cone	$A = \pi h_p^2 tan^2\theta$	α	α	0.727	1

It is important to select the correct tip for each application in order to offer high precision that enables finest quality data for intended research. Nano indentation instruments unlike other laboratory infrastructure are relatively easy to use, their controls are computerized and it does not require vacuum chambers or expensive laboratory infrastructure. The technique requires the ability to understand and to precisely manipulate and use the results in for useful purposes. The benefits can be of great benefit in the manufacture of medical devices, consumer goods, machine tools and even in automotive industry.

CHAPTER 3

EXPERIMENTAL PROCEDURE

3.1 Material Description

The materials examined in this study were the single crystal silicon wafer doped with boron (100), tungsten carbide, A2 and D2 tool steels. The tool steels were acquired from McMaster- Carr (Atlanta, GA USA) in annealed condition. Fused silica was used as a standard specimen to determine the area coefficient of different indenter tips geometry using the Analytst^{TM} software. The nominal elastic modulus of fused silica is 72 GPa.

Fused silica has some unique properties that make it ideal for calibration standard specimen in nanoindentation testing. These properties include:

- No significant time dependence
- Readily available and inexpensive to obtain in bulk form
- Mid-range mechanical properties

Table 3.1: Chemical composition of A2 and D2 tool steels in wt. %.

Steel	Composition in wt. %					
	C	Mn	Si	Mo	Cr	V
D2	1.55	0.4	0.3	0.8	12.00	0.8
A2	1.0	0.6	0.3	1.10	5.5	0.2

Table 3.2: Mechanical properties of A2 and D2 tool steels.

Nominal Density, lbs./cu.in.	Modulus of Elasticity, GPa	Thermal Conductivity Btu/sq.ft./ft./hr/^{0}F @ 212^{0}F	Tensile Strength, Ksi	Yeild Strength, Ksi	Elongation %
A2: 0.28	207	7.91 x 10^{-6} (200^0 to 1200^{0}F)	Anneled:70-103 Quenched: 253	Annealed: 51 Quenched: 200	Annealed: 26 Quenched: 1
D2: 0.28	210	5.7 -7.4 x 10^{-6} (68^0 to 75^{0}F)	Quenched: 278	Quenched: 214	1

Table 3.3: Mechanical properties of silicon wafer [100].

Property		Value	Units
Bulk modulus of elasticity		$9.8 \cdot 10^{11}$	dyn/cm^2
Density		2.329	*g/cm^3*
Hardness		7	on the Mohs scale
Surface microhardness (using Knoop's pyramid test)		1150	*kg/mm^2*
Elastic constants		$C_{11} = 16.60 \cdot 10^{11}$	*dyn/cm^2*
		$C_{12} = 6.40 \cdot 10^{11}$	*dyn/cm^2*
		$C_{44} = 7.96 \cdot 10^{11}$	*dyn/cm^2*
Young's Modulus (E)	[100]	129.5	*GPa*
	[110]	168	*GPa*
	[111]	186.5	*GPa*
Shear Modulus		64.1	*GPa*
Poisson's Ratio		0.22 to 0.28	
Fracture toughness		0.95	$\mathrm{MPa} * \sqrt{\mathrm{m}}$

Tools steels as the name suggests are steel made into tools for purposes like cutting, shaping and forming of materials in definite shape for specific needs. Previously, tools steels were made of plain carbon which was limited in its application but increasingly from 19th century, complex and high alloyed ones have been developed in order to meet the varying demands on engineering structures and products as technology continues to move away from conventional to sophisticated applications. Robert Mushet in 1868 pioneered the concept of alloying when he added tungsten to high-carbon steel; his alloyed steel was well known to harden in air cooling after heat treatment and was considered as the first high-speed steel. With the discovery of chromium in 1797 [34], alloying with chromium was first claimed in an America patent filed by Julius Baur in 1876. Around 1894 to 1894, Taylor and White discovered at elevated temperature heating above the range common within that time and subsequent air cooling of chromium-tungsten steels could produce a tool steel that can exceptional hardness even at red heat.

Tool steel has to be heat treated in part or whole in order to obtain the desired properties like wear resistance, toughness, deformation resistance at high temperature, fracture under high loads and softening at elevated temperature. The start of the new century saw increase activities in heat treatment and development of high-speed steels, metallographic advances, use of x-ray to examine materials and scientific understanding of phase transformation and microstructures [35, 36] which was a huge contribution to the overall field of alloys tool steels. Tool steels are combination of high-quality steel chemically branded together under careful selected conditions in order to obtain specific mechanical properties and tolerances. The combination of alloying elements like tungsten, molybdenum, vanadium and

chromium makes it possible for these alloys to withstand severe service conditions while it offers dimensional control and resistance to cracking during heat treatment. Is important to note that no single tool material possesses all the desired properties like wear resistance, toughness and etc., therefore for a particular tool material, there is often a need for a tradeoff to achieve the optimum combination of properties.

3.2 Heat Treatment

According to HTSE (International Federation of Heat Treating and Surface Engineering) heat treatment is defined as "a process in which the entire object, or a portion thereof, is internationally subjected to thermal cycles and if required, to chemical and physical actions, in order to achieve desired (change in the) structures and properties" The term thermal cycle mentioned above are the different heat treatment steps like: stress relieving, austenitizing, normalizing, annealing, quenching and tempering employed in order to achieve the desired result. The purpose why steel undergo heat treatment is to improve their ability to be machined and mechanical properties (like yield strength, resistance to corrosion, tensile strength and creep performance), increase their strength and toughness, release residual stress, and prevent crack and control of its microstructure. The specific purpose/desire for heat treating steels determines the necessary steps to follow in order to achieve the intended result. In order to predict the microstructure formation during heat treatment, ITD (isothermal transformation diagrams) alias TTT (time-temperature-transformation) curves, and CCDC continuous coiling diagrams) alias CCT (cooling time-transformation) curves are used.

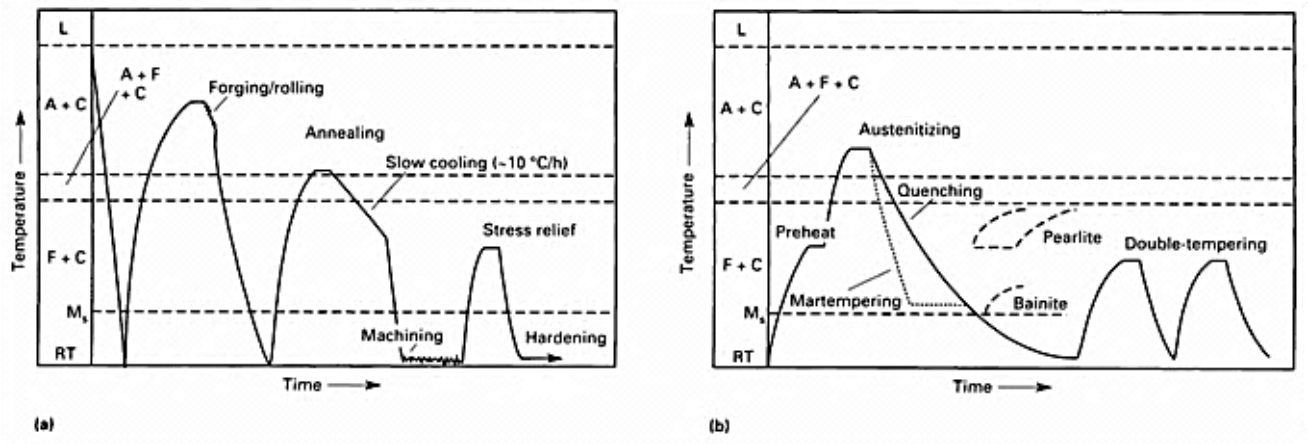

Fig. 3.1 Plots of temperature versus time showing sequence of operations required to produce tool steels. (a)Thermomechanical processing (b) Hardening heat treatment. L, liquid; A, austenite; C, cementite; F, ferrite; M_s, temperature at which martensite starts to form on cooling; RT, room temperature [37].

In heat treatment of steel, the first step is to heat the steel to its austenitizing temperature. Austenitization is the process of forming austenite by heating the steel above the critical temperature in order for the formation to take place. In order words, the complete transformation of steel to austenite is known as austenitization, this process is the most important heating operation performed on steel.

In the austenitization process, the heat rate and holding time are very vital variables. A particular heat rate has to be maintained in order to prevent cracking in the material. This is important since steel at 200 – 600° C temperature range lacks sufficient plasticity to accommodate increased thermal stresses.

The heating rate depends on:

1. Size and shape of the component
2. Initial microstructure
3. Steel composition

Steel's tendency to develop crack is based on its carbon composition. The potential for crack initialization base on the effect of its carbon composition can be calculated modally with carbon equivalent (C_{eq}) using this equation:

$$C_{eq} = C + \frac{M_n}{5} + \frac{C_r}{5} + \frac{M_o}{3} + \frac{N_1}{10} + \frac{V}{5} + \frac{S_i - 0.5}{0.5} + \frac{T_1}{5} + \frac{T_1}{5} + \frac{W}{10} + \frac{AL}{10} \quad (13)$$

The elements are represented in wt% concentration in the steel. The following limits exist for the equation:

$C \leq 0.9\%,\ Mn \leq 1.1\%,\ Cr \leq 1.8\%,\ Mo \leq 0.5\%,\ Ni \leq 5.0\%,\ V \leq 0.5\%,\ Si\ \leq 1.8\%, Ti \leq 0.5\%, W\ \leq 2.0\%\ and\ AL \leq 2.0\%.$

The C_{eq} value shows the possibility for crack to develop with the steel. LISCIS [41] reported the following general rule:

C_{eq} ≤ 0.4: Steel not sensitive to cracking, may be heated quickly.

C_{eq} = 0.4 – 0.7 Moderate sensitivity to cracking.

C_{eq}≥ 0.7 Potential of crack in steel is high, the steel should be preheated to a temperature close to AC_1 (the temperature at which austenite begins to form during heating) and held until an even distribution is attained in order to reduce thermal stressed when austenitizing.

The microstructure and hardness of steel determines how heat is applied, steel without a uniform microstructure and with high hardness should be heated slowly than steel which possess a uniform microstructure and low hardness. The grain size increases with increase in austenitization temperature. It is important to note that the tendency for brittle fracture to occur in steel increases with growth in grain size therefore is important to select the right austenitization temperatures to provide the best hardness and grain size which subsequently influences the heat treatment and steel performance under working conditions. The best

austenite temperature could be considered as the temperature where hardness is highness and the grain size finest.

A general rule for proper estimation of the appropriate soaking time during austenitization is given by $T = 60 + D$ where T, represents the soaking time in minutes and, D, is the maximum diameter of the component in millimeter. Factors that can influence the soaking time includes; the thermal properties of the load, and furnaces emissivities, initial furnace and load temperature, characteristic fan curves, and composition of the furnace atmosphere. The processing information and service characteristics of A2 and D2 tool steels are shown in Table 3.4 and Table 3.5:

Table 3.4: Hardening and tempering of A2 and D2 tool steels.

Type	Rate of heating	Hardening				Time at temperature, min	Quenching medium[(a)]	Tempering temperature	
		Preheat temperature		Hardening temperature					
		°C	°F	°C	°F			°C	°F
Medium-alloy air-hardening cold work steels									
A2	Slowly	790	1450	925–980	1700–1800	20–45	A	175–540	350–1000
High-carbon, high-chromium cold work steels									
D2	Very slowly	815	1500	980–1025	1800–1875	15–45	A	205–540	400–1000

(a) O, oil quench; A, air cool; S, salt bath quench; W, water quench; B, brine quench.

Table 3.5: Processing and service characteristics of tool steels.

AISI designation	Hardening and tempering					Fabrication and service			
	Resistance to decarburization	Hardening response	Amount of distortion[(a)]	Resistance to cracking	Approximate hardness[(b)], HRC	Machinability	Toughness	Resistance to softening	Resistance to wear
Air-hardening medium-alloy cold work steels									
A2	Medium	Deep	Lowest	Highest	57–62	Medium	Medium	High	High
High-carbon, high-chromium cold work steels									
D2	Medium	Deep	Lowest	Highest	54–61	Low	Low	High	High to very high

Source [60].

3.3 Microstructure and Mechanical Property Relationship in Tool Steels

Altering the microstructures of steel is the backbone behind the wide range of properties generated from it. The use of different approaches to heat treat and varying the thermochemical process in manufacturing of given steel has been exploited to control microstructural changes thereby resulting in properties variation in steel products. There are tool kinds of steel: low-strength/high-ductility/high toughness or high-strength/high-fatigue-resistance/low-toughness categorize according to the carbon content.

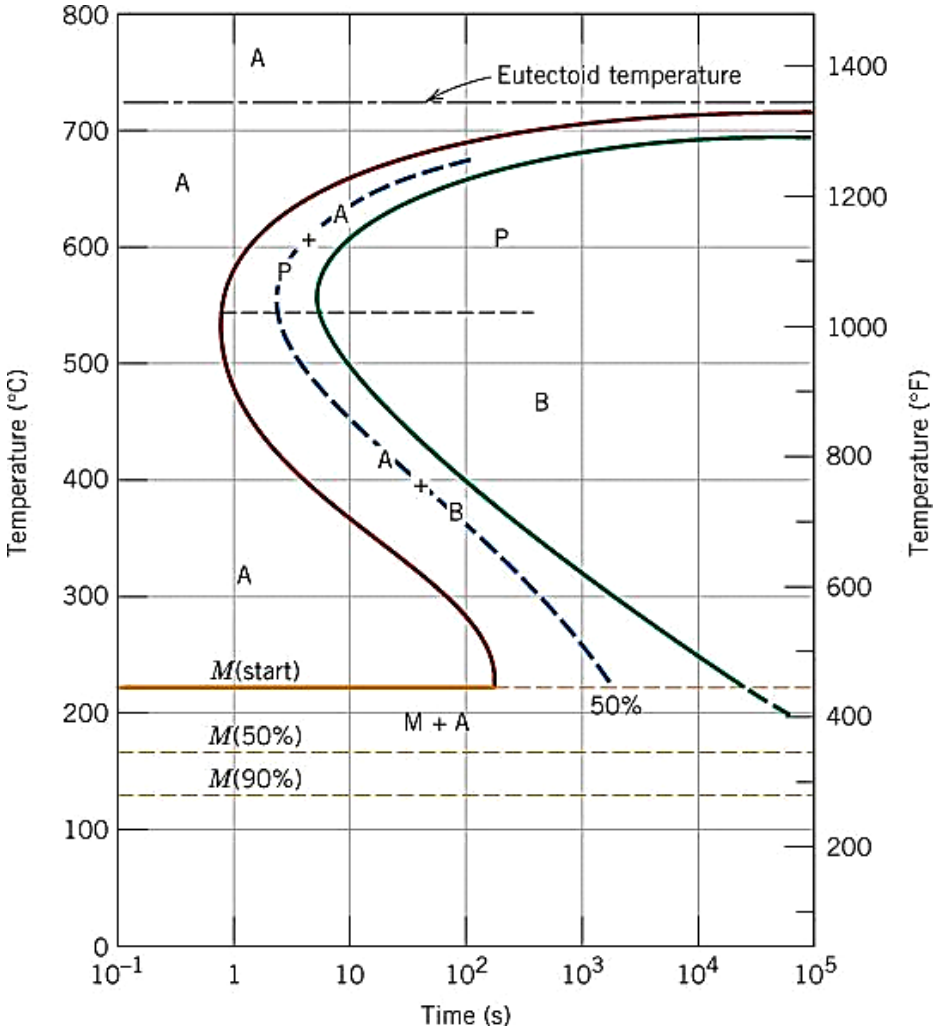

Fig 3.2. Isothermal transformation diagram [A: austenite, P: pearlite, B: bainite, M: martensite]

Factors that play key roles in the performance of steel properties for a given composition in a given processed condition are linked to microstructures which involve the volume fraction, sizes and the various phase morphologies of the steel. Heat treatments, cold deformation, solid-state phase changes and hot deformation are used blend the all the crystal phases present in the steel microstructures. For every microstructure and the resulting product, the defining characteristics property ranges are controlled by manipulation of the processing route in other to exploit the microstructural changes. A vital component in respect to microstructure evolution is to know the different processing route to which different types of steels are subjected. The main component of steel is iron. Below its melting point, it exists in two crystal forms.

(1) The α-ferrite, body-centered cubic (bcc) that is stable from below room temperature to 912°C (1675°F) and from 1394°C (2540°F) to melting point 1530°C (2785°F). The higher temperature range is known as the δ-ferrite.

(2) The austenite or γ-iron which is face-centered cubic (fcc), stable between 912 and 1394°C (1675 and 2540°F).

Steels do contain carbons which profoundly change their phase relationships, microstructure and properties. The carbon contents are kept low in steels that require high ductility, high toughness and good weld ability however in cases where high wear resistance, high strength, high hardness, fatigue resistance are required the carbon content are generally high. The presence of carbon in the iron-carbon phase diagram is to act as an austenite stabilizer and it expends the temperature range of stability of austenite. Carbon solubility in ferrite and austenite is a function of temperature, if the octahedral interstitial sites between the iron atoms gets full and could not accommodate more carbon atoms between iron atoms; a new phase will be form in order to accommodate more carbon atoms in its crystal structure.

The new orthorhombic crystal structure phase formed is called the cementite (Fe_3C). It is this formation of the cementite phase and carbon solubility in austenite and ferrite as a function of temperature controlled by alloying and processing that accounts for the wide variety of microstructures and properties in steels.

Steels contain up to 2.00 wt. % C and the basis for hot workability and heat treatment of carbon steels is the austenite phase. The single austenite phase is readily hot-worked. Upon cooling, austenite transforms to other microstructures. When the cooling rate is slow under conditions approximating equilibrium, austenite transforms into a mixture of ferrite and cementite; when the cooling rate is quick, a martensite is form. The heat treatment of steels is based on these transformations. In effect, the high stability of the austenite phase at elevated temperature in iron and iron-carbon alloys and the solid-state transformation of austenite upon cooling accounts for the great chances to utilize microstructures, section size, optimize shape and properties in many applications. The different phases that could be formed at various temperatures define the processing critical temperature for the formation and transformation of austenite. The critical temperature is dependent on the carbon content; it can be identified as changes in slope or thermal arrests in heating and cooling curves. Equilibrium, heating and cooling conditions all affects the critical temperature designation boundary on the iron-carbon phase diagram. The additions of other alloys like nickel and manganese which are austenite stabilizers also lower the critical temperatures while the silicon, chromium raises the critical temperature and shrinks the ferrite austenite phase.

Obviously, different types of microstructures increase strength with increasing carbon content with the expectation of low-carbon steels that do not have enough hardenability to

form martensite. The highest level of increases is seen in the martensite phase because of the low carbon solubility in ferrite. This accounts for the significant effect of the ferrite matrix grain sizes and morphology on the mechanical behavior at any given carbon level.

Martensite phase produces the highest level of hardness and strength in steel. The martensitic transformation involves the sudden reorientation of C and Fe atoms from the FCC solid solution of $\gamma - Fe$(austensite) to a body-centered tetragonal (BCT) solid solution (martensite). It's the diffusionless transformation of austenite which occurs upon cooling, cooling rates that is so rapid enough to suppress the diffusion-control transformation of austenite to ferrite, pearlite and bainite. The deformation of the martensite is called the lattice invariant deformations or twins in martensite. This fine structure and the carbon atoms trapped within the octahedral interstitial sites of the body-centered tetragonal structure, produces the very high strength of as-quenched martensite [40]. The formation of martensite starts at the martensite start (Ms) temperature which is a critical temperature, it involves nucleation and growth of many new crystals before the transformation takes place. It is an athermal transformation, no thermal activation is needed. The strength of martensite is not a result of its microstructure but is due to the interstitial C atoms hindering dislocation motion and to the small number of slip systems.

3.4 Microstructural Analysis and Application of D2 Tool Steel

D-types of tool steels have high-carbon and high-chromium; they were designed to be used in place of high-speed steels. Their resistance to wear can be linked to its high carbon and alloy contents which produce large volume fractions of high-hardness alloy carbides for cold-

work applications. [52-54]. D-type material has high hardenability and deep-hardening characteristics due to slow diffusion-controlled transformation of austenite by high alloy element content. Molybdenum is normally added to D-type steel to suppress the formation of pearlite. During forging process of D2 materials, temperature is kept within the range to prevent partial dissolution since steel of this type becomes molten at 1150°C (2100°F). D-type material has to be heated gently in a uniform manner to austenitizing temperature to be able to exploit fully its dimensional stability because it is important for the production of hardened microstructures of high hardness. The hardening stage involves heating to the austenitizing temperature holding at the austenitizing temperature and then quenching. Tool steel is heated in neutral atmosphere to maintain surface carbon contents. Proper austenitizing of high-carbon, high-chromium tool steels is important in the production of hardened microstructures of high hardness. Each tool has a particular temperature for achieving the maximum hardness which is determined by the optimum solution of the alloy carbides in annealed microstructures. D2 tool steel which is considered as a low carbon type have reasonable higher wear resistance and possess slightly higher toughness than other D type containing 2% of carbon or more.

3.5 Microstructural Analysis and Application of A2 Tool Steel

The ultimate goal of applying heat treatment to tool steels ideal is to obtain high hardness and mircostructures that have have high hardness. The highest hardness attainable in a tool steel is linked to martensite mircostructure formation and the retained austensite in the high-carbon steels. Chemical compostion, crystal structure and perfection, the size and distribution of the various phases present in the microstructure all determine the hardness of a

material. Since A-type tool steels are suspectible to decarburization during austenitizing transformation for hardening, a high austenitizing temperature will result in lower hardness because excess austenite will be retained in the hardened microstructure while a low austenitizing temperature will cause a formation of nonmartensitic microsturucture during air cooling which will result in lowering hardenability. Austenitizied at 1740°F (950°C), a hardness of 63 to 65 HRC could be obtained for a air-cooled quenching. A-type tool steel can be used for punches, feel rolls, gages, forming dies, drills, circular cutters and burnishing tools.

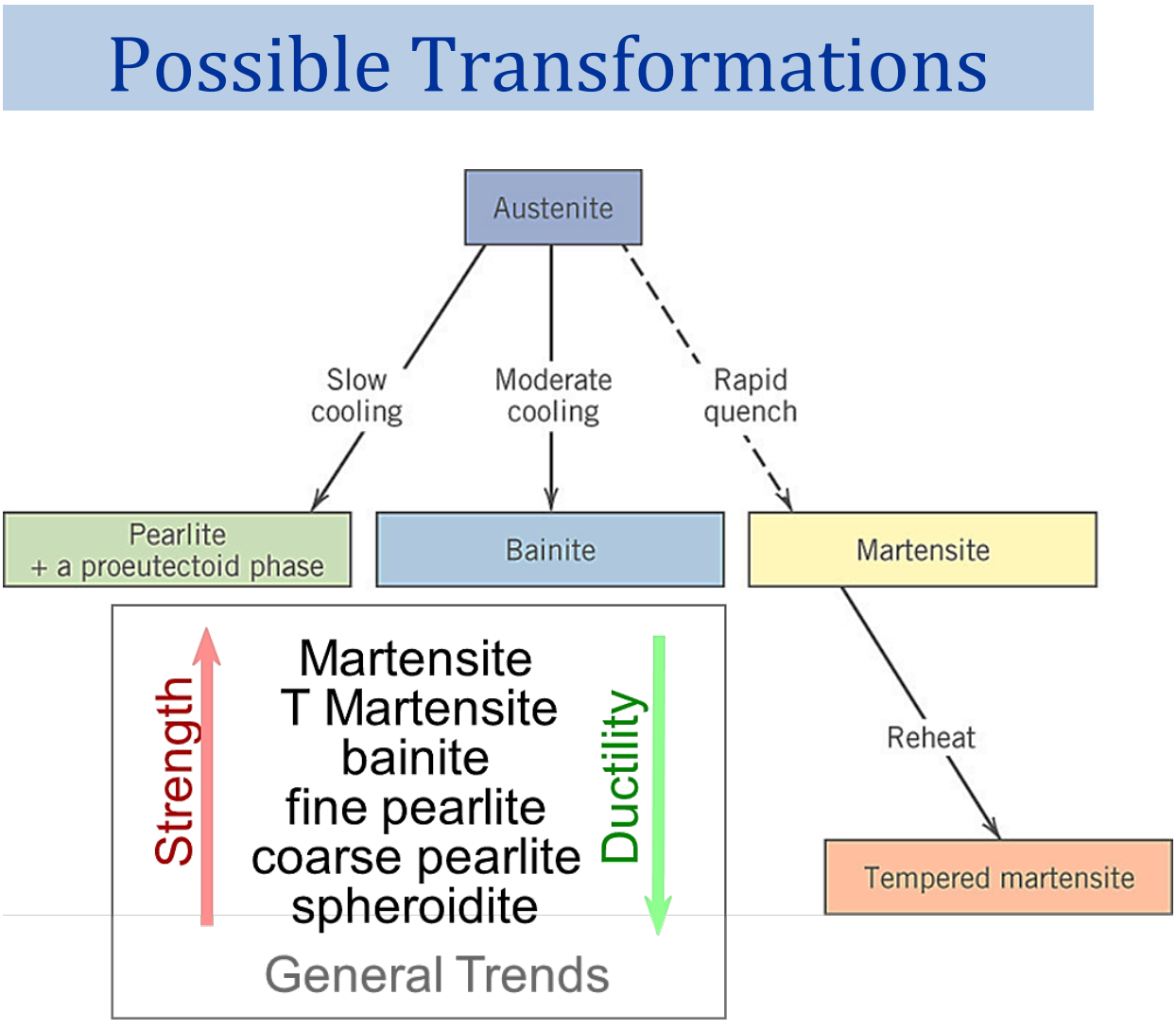

Fig. 3.5. Summary of austenite transformations

CHAPTER 4

SPECIMEN PREPARATION

4.1 Grinding and Polishing

Sectioning of examined samples was done with a low-speed wheel blade softly bonded with diamond girts to avoid burning the material surface. D2 tool steel was received in the form of metal strip with cross-section of 3.14 x 12.7 x 12.7mm. A2 came in rod form with cross-sectional diameter of 12.7mm. The samples were polished manually using a polishing stage at 250 rpm to remove surface scratches and deformations from cutting. Polishing was done with the application of heavy to moderate pressure for about 30 minutes to one hour. The grades of abrasive paper used for the polishing increased in sequence of 240, 400, 800 and 1200 grits. Final polishing was done using a 0.05µm γ-alumina (Al_2O_3) suspension on a soft cloth. Colloidal silica suspension of particle size of 0.04µm was also used for polishing to minimize strain hardening of the sample surface. The Rockwell hardness values were obtained for all the samples (A2 and D2) after polishing. The specimens were labeled (a) as-received, (b) heat treated and air cooled and (c) heat treated and water quenched for both A2 and D2 tool steels respectively.

4.2 Hardening Process

No heat treatment was carried out on the as-received specimens of A2 and D2 tool steels. The heat treatment for specimens (b) and (c) was carried our accordingly and the temperature readings were obtained using a laboratory thermo couple. Specimen (b) of A2 tool steel was preheated thoroughly at 1450-1500°F, then raised to a hardening temperature of

1800°F and held at this temperature for about 30 minutes, then quenched in still air immediately. Subsequently, specimen (b) of D2 tool steel was preheated to 1200°F and held at that temperature until thoroughly soaked. Then heated to 1850°F and held at this temperature for about 30 minutes. The specimen was removed from the furnace and quenched in still air immediately. Specimens (c) of A2 and D2 tool steels were heat treated in the same manner as mentioned in specimens (b) above for A2 and D2 tool steels respectively, but was quenched in water mixed with ice (temperature of water after mixing with ice was 50°F and the ambient temperature was 67.3°F) after heat treatment. After heat treatment and quenching, the HRC values of specimens (b) and (c) for A2 and D2 tool steels were measured using Rockwell hardness tester [Wilson Mech. Inst. Division] to determine the influence of heat treatments. Mechanical properties of materials are evaluated for only locations that come in contact with the indenter.

4.3 Metallography

Metallographic images of the specimens were obtained after etching the sample surfaces with 2% nital. Nital is a combination of nitric acid and alcohol; for this research work the composition of nital used comprise of 2% of Nitric acid and 98% alcohol. The etching was performed by immersion. Trial and error methods are used to determine the length of time that gives the best result because tool steel composition and the heat treatment can alter the etching response. Once the degree of dulling needed to establish the microstructure clearly is attained, the etchant was thoroughly washed off with water from the sample and dried with a

warm air. The exposed structures were examined and the metallographic images were obtained using optical microscope.

4.4 Surface Roughness and Friction

In the test of buck materials, like in this case of tool steels, surface roughness is a challenge since it can lead to large errors in the contact areas [16] that are used in determining the mechanical properties. To avoid the occurrence of interference the distance between successive indentations are kept at 50 microns which is at least 20 to 30 times the maximum penetration depth when a Berkovich indenter is used. The hardness result from indentation result is affected more by surface roughness than the elastic modulus because in area hardness determination, the area term is used directly but in calculation of elastic modulus the square root of the area is used [61]. The measured mechanical properties at the minimum penetration depth, h_{min}, is given by $h_{min} = \frac{Surface\ Roughness}{0.05}$

The effects of friction in indentation test have been studied in many research works, Yurkov et al (1997) noted that the sliding coefficient of friction of diamond on various surfaces such as steel, fused silica and alumina is not constant but is dependent on the load. The coefficient is assumed to be zero due to the fact that it has small influence on the result. Since the coefficient of friction of diamond on metals and fused silica is similar, we will assume that friction will have no effect on the test.

4.4 X-Ray Diffraction

X-Ray diffraction technique is a non-destructive means used to measure the structural

properties like crystal orientation, phase orientation, grain size, phase composition and stress. X-Ray diffraction is used to determine the crystal structure of a material by comparing the generated diffraction pattern with reference patterns. Rigaku Ultima III diffractometer was used in the parallel beam mode with a buck material stage and a scintillation detector to determine the grain size of the specimens in this study. The x-ray source and the detector are placed on circumference of the diffracting circle with a projection angle of 2θ between the x-ray source and specimen. X-rays are produced in evacuated x-ray tube by directing an electron beam of high voltage at metal anode. The target metal determines the operating voltage. The diffracted x-ray source passes through a series of slits called soller slits which defines the incident beam. After the beam has been diffracted from the specimen, it passes through another set of slits which produces the radiation of the beam representing different intensities. The position of the peaks depends on the crystal structure of the sample with allowed reflections on fcc and bcc metals.

Using Debye-Scherrer equation,

$$d = \frac{0.9\lambda}{\beta cos\ \theta} \qquad (14)$$

the grain size of each specimen of A2 and D2 tool steel were obtained according to Bauer et al., 1978 method. λ in the equation is characteristic wavelength of 0.154nm, β is the full-width at half maximum (FWHM) of the broadened diffraction line on the 2θ scales (radians) and the θ is the angle (Bragg angle) between the incident beam and sample plate in the XRD machine. The FWHM of the instrument used obtained from x-ray diffraction spectrum of single crystalline Si wafer is 0.0016049 (radians). Thus if the observed peak of the material has width of W_{FWHM} and

the width due to instrumental effect is $W_{instr,}$ then the new width used in determining the crystallite size W_{sample} is given by: $W_{sample}^2 = W_{FWHM}^2 - W_{instr}^2$ (15)

4.5 Nanoindentation

In order to in investiage the influence of heat treatment on the specimens, series of experimental indentations was performed with the Berkovich indenter tip in order to obtain a qualitative estimation of heat treatment and quenching influence on hardness (H) value and elastic modulus (E) during unloading as observed in the present study. Series of indentation experiments was performed on each specimen and the maximum depth was kept at 10% of the sample size to minimize the effect of pile-up. The process involves pushing the indenter gently into the surface of the specimen which causes both elastic and plastic deformation to occur; a contact area that conforms to the shape of the indenter is produced after the indenter is withdrawn from the specimen. The hardness, H and effective elastic modulus, E_{eff} was obtained from these fundamental relationships:

$$H = \frac{P_{max}}{A} \quad (16)$$

$$E_{eff} = \frac{1}{\beta}\frac{\sqrt{\pi}}{2}\frac{S}{\sqrt{A}} \quad (17)$$

where P_{max} is the maximum load, A is the projected contact area and β = 1.034, a constant dependent on the geometry of the indenter for the Berkovich indenter tip. Elastic modulus was computed using the effective modulus equation

$$E_{eff} = \frac{1-V_i^2}{E_i} + \frac{1-V^2}{E} \quad (18)$$

where E and v are the Young's modulus and Poisson's' ratio for the specimen, and E_i and v_i are the same for the indenter. E_i = 1141 GPa, v_i = 0.07 and v = 0.3 (Olivier and Pharr, 2004), with about 5% uncertainty.

Analysis of a typical nanoindentation test method:

1. The indenter approaches the test surface until contact is realized. Contact is determined by an increase in stiffness relative to the indenter column's support springs. Approach rate and stiffness increase criteria are user specified.
2. The indenter is driven into the surface until the maximum force or penetration depth is reached. The rate at which the indenter is pushed into the material and the displacement or force limit is user defined.
3. The force is applied to the material is held constant for a period of time determined by the user. This dwell time is implemented for materials that experience small amount of creep. At the end of the dwell time creep should be negligible.
4. The indenter is withdrawn from the material at a rate equivalent to the loading rate until the force reaches 10% of the peak force.
5. The force applied to the material is held constant for a user specified period. This test segment is used to determine the drift rate or the thermal drift rate experienced by the material. If the drift rate is small in relation to the overall penetration depth, this segment is not required.
6. The indenter is withdrawn from the sample.

CHAPTER 5

RESULTS AND DISCUSSIONS

5.1 Rockwell C Scale Hardness (HRC)

The HRC values of all examined samples were obtained after the hardening process. Hardening of steel requires a change to occur in its structure. As already discussed when steel is heated to the austenitic temperature and suddenly quenched, the martensitic structure is formed. This structure is very strong and brittle in nature. This is reason why some samples of A2 and D2 tool steel were quenched in water.

The Rockwell C hardness results reveals on a macro scale how the hardening process affects the microstructure, grain size, the dissolution of carbide plus other mechanical properties like hardness. Table 5.1 shows the hardness values (HRC) for A2 and D2 tool steel hardened by air cooling and water quenching. We presumed that since D2 tool steel has higher carbon content than A2 tool steel (Table 3.1); its hardness value is expected to be higher than that of A2 tool steel since hardness is a function of the carbon content of the steel. However this is not the case, the hardness value (HRC) of A2 tool steel is slightly higher that than of D2 tool steel. This difference could be explained by the presence of some alloys like Molybdenum in A2 tool steel. A higher Molybdenum content in A2 tool steel (wt. % 1.10) can effectively suppress the formation of pearlite (less harder microstructure) which can conversely result in the formation a harder microstructure. However, in practice the lower hardness (HRC) value of D2 tool steel makes it more resistant to wear than A2 tool steel.

Table 5.1: HRC values for all tested samples:

Steel	Rockwell Hardness Test, HRC		
	As received	Heat treated and Air cooled	Heat treated and water quenched
A2	22.5	62.1	63
D2	15	61.9	62.1

5.2 Metallography

Before heat treatment, the samples of A2 and D2 tool steel were etched and observed under a scanning electron microscope. As shown Fig. 5.1 and Fig. 5.2, large amount of carbides are present in the as received tool steels in annealed condition. These carbides supply to the austenite carbon necessary to achieve hardness during the hardening process.

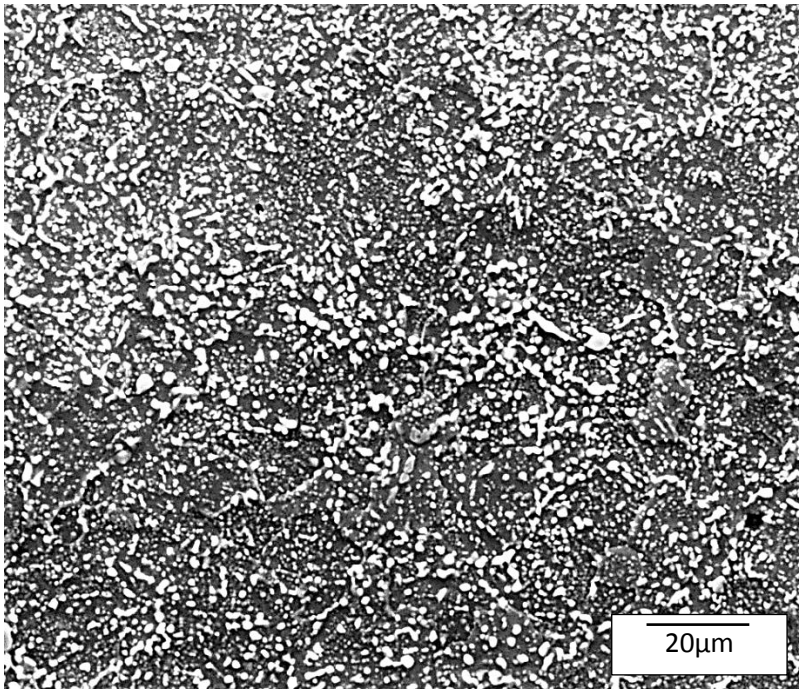

Fig. 5.1. Microstructures of A2 “as received” tool steel samples in annealed condition [20µm]

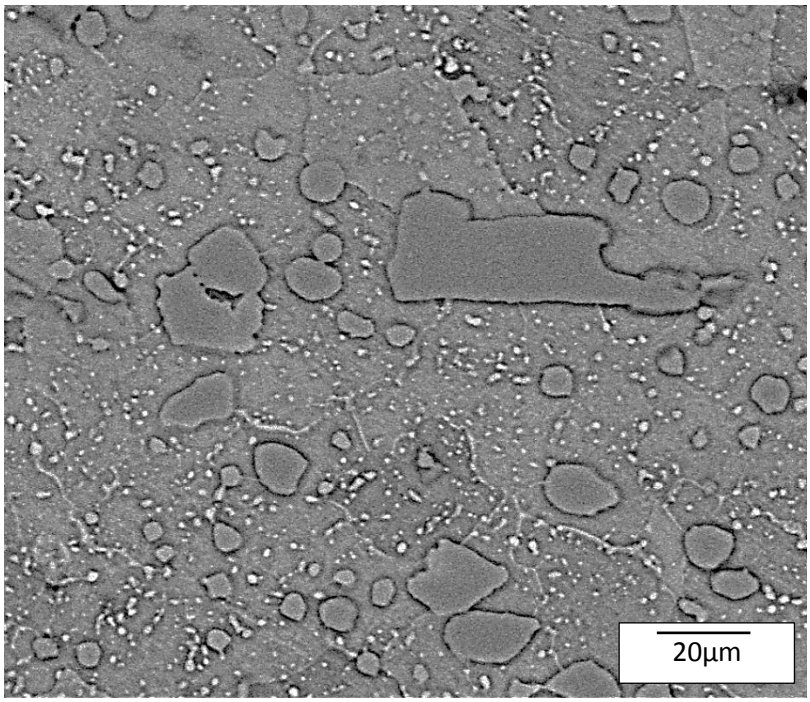

Fig. 5.2. Microstructures of D2 “as received” tool steel samples in annealed condition [20µm]

The microstructure of the as-received specimens showed the distribution of coarse and fine spheroidized carbide particles in a matrix of ferrite grains, which are highly machinable and offer less resistance to deformation when compared to other microstructures formed in hardening of tool steels. The larger particles of the distributed spheroidized carbides seen in Fig. 5.2 are primary M_7C_3 carbides formed during solidification which got dispersed as a result of hot working, the finer carbides are as a result of secondary precipitation in the spherodiziation of carbides produced by the transformation of austenite to ferrite-carbide microstructures on cooling after earlier normalizing heat treatments. During heat treatment the carbides provides the austenite the carbon for hardness to be attained, but it is necessary to have some retained carbides. These retained carbides contribute significantly to wear resistance during service. The carbides seen in Fig 5.3 are primary alloy carbides that do not dissolve even during high-temperature austenitizing of A-type steels. The smaller dissolved

carbides Fig. 5.4 during austenitizing accounts for the increase in the hardening value in tool steels. The amount of carbides present in tool steels reduces after quenching; this is because carbides supply the austenite the required carbon necessary for hardening.

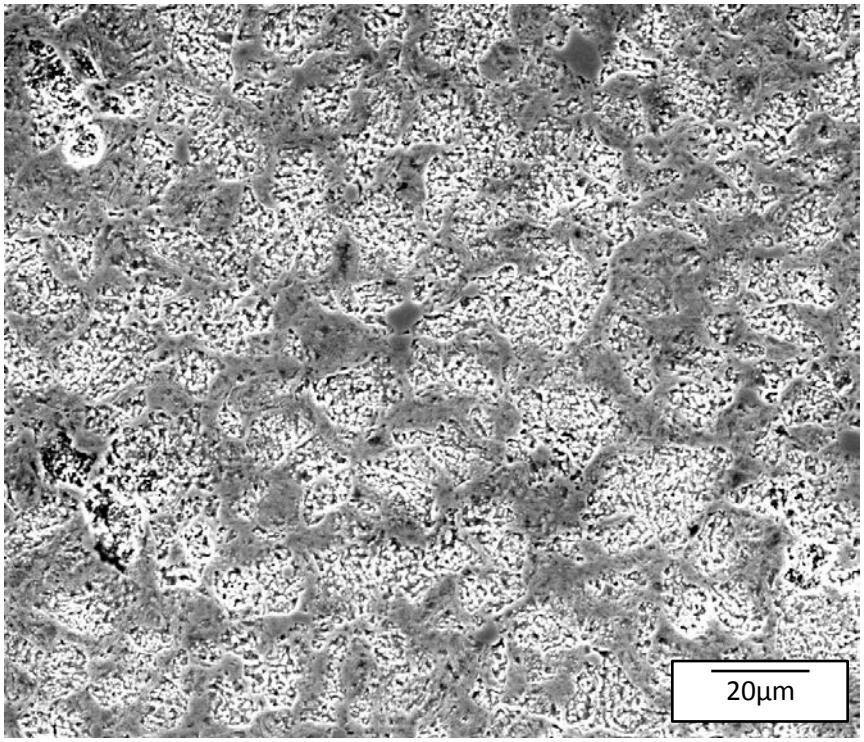

Fig 5.3. Microstructures of A2 “heat treated and air cooled” tool steel sample [20µm]

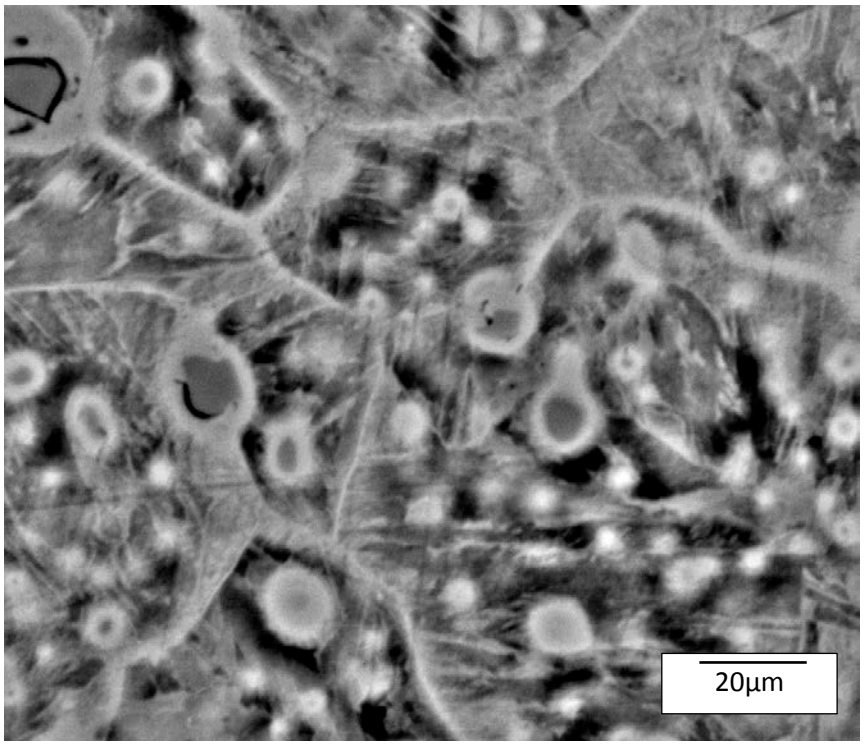

Fig 5.4. Microstructures of D2 “heat treated and air cooled” tool steel sample [20µm]

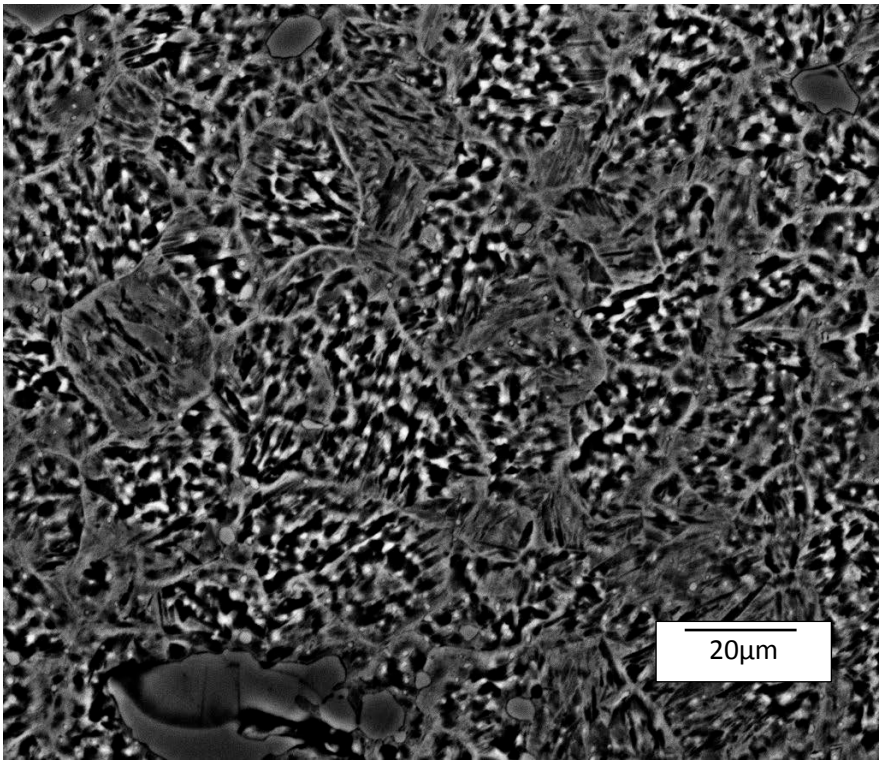

Fig 5.5. Microstructures of A2 “heat treated and water quenched” tool steel sample [20µm]

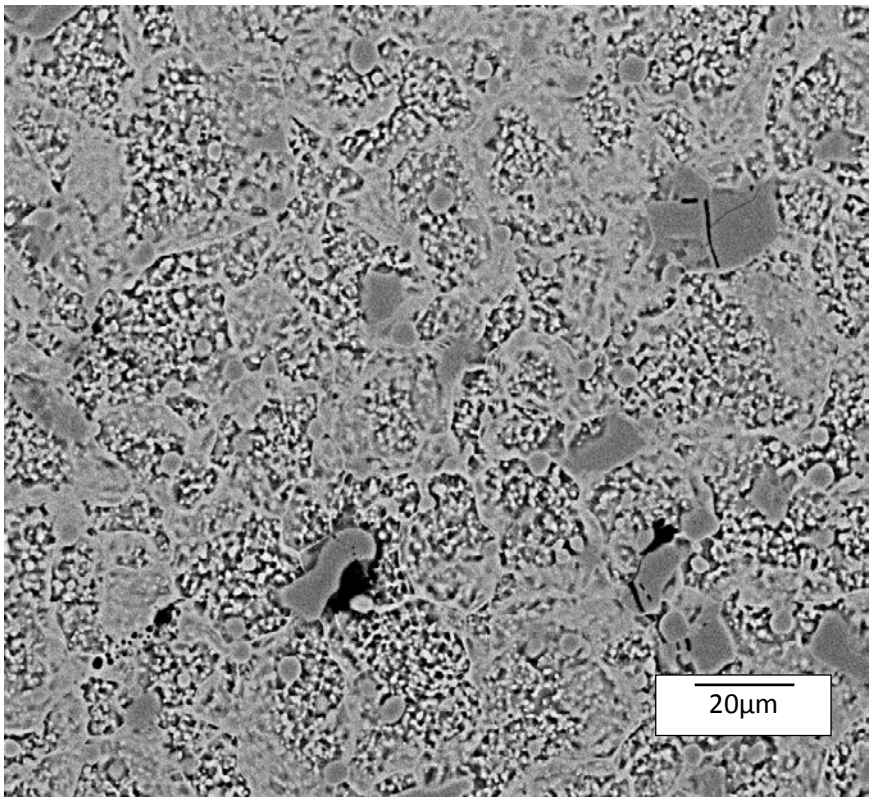

Fig. 5.6. Microstructure of D2 “Heat treated and water quenched” tool steel sample [20µm]

5.2 X-Ray Diffraction

Since the XRD experiment provides a more detailed explanation of how the microstructures have been affected by heat treatment, results from XRD analysis for all test samples are reported below.

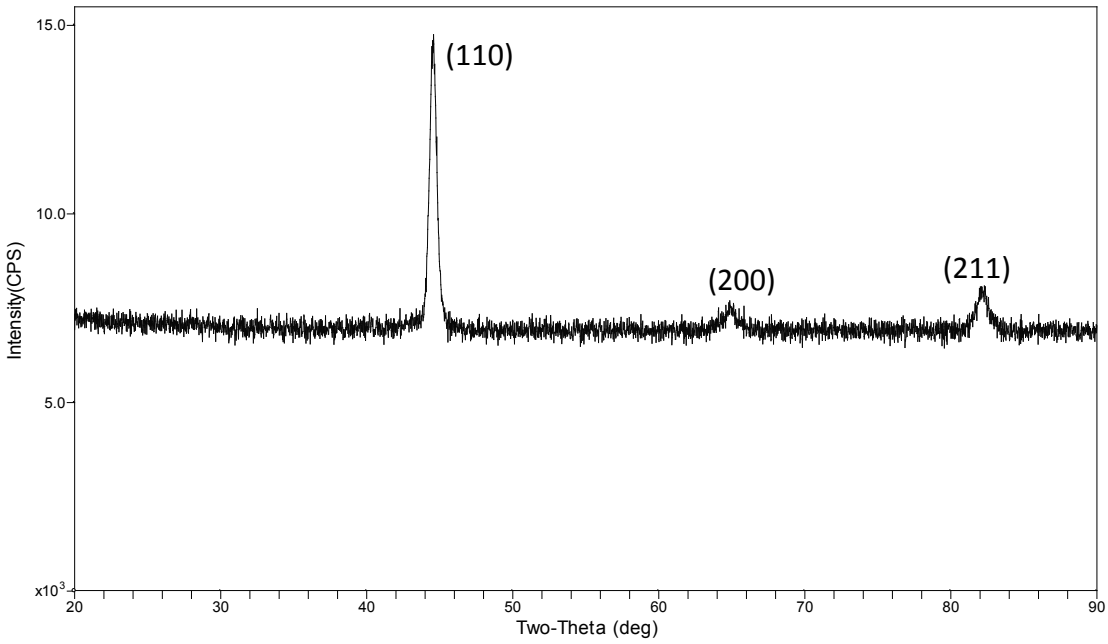

Fig 5.7. XRD pattern of A2 tool steel sample (heated treated and water quenched)

The crystalline grain size, d, of A2 tool steel sample (heat treated and water quenched) from the observed peak intensity of the XRD diffraction is given by:

$$W_{sample}^2 = W_{FWHM}^2 - W_{instr}^2$$

$$W^2 = (0.31)^2 - (0.09)^2$$

$$W = 1.3069\ (0.022\ radians)$$

$$d = \frac{0.9\lambda}{\beta cos\ \theta}$$

$$d = \frac{0.9 * 0.154}{0.022 * 0.9255} = 6.81nm$$

λ in the equation is characteristic wavelength - $0.154nm$, $0.9255 = \cos\theta = [\ 2\theta = angle\ at\ max.intensity, therefore\ \theta = \frac{angle\ at\ max.intensity}{2}\ ]$

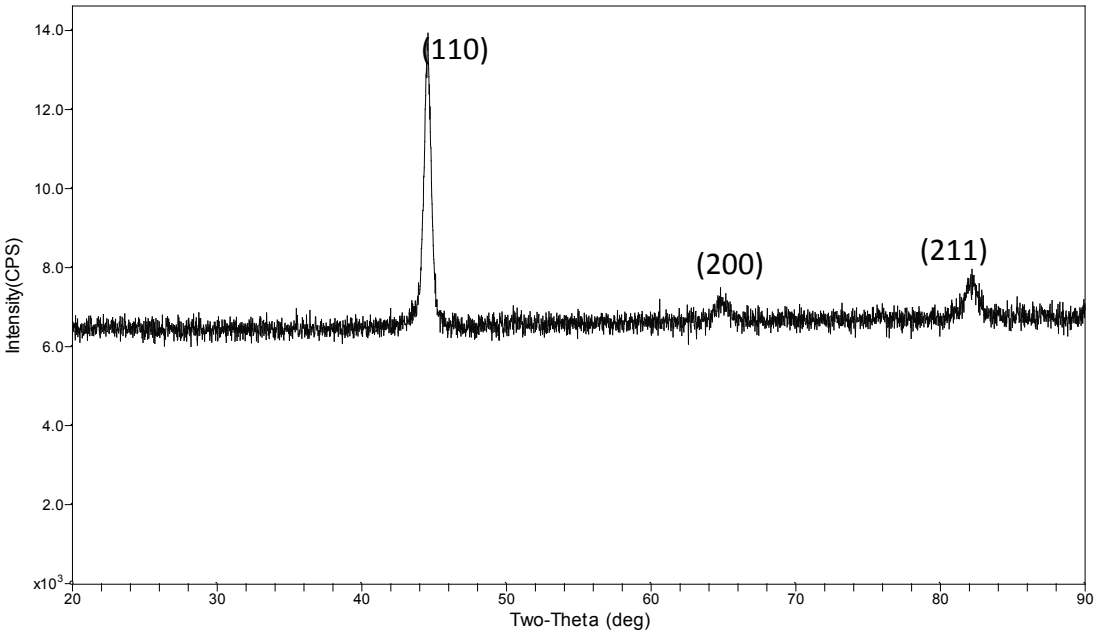

Fig 5.8. XRD pattern for A2 tool steel sample (heat treated and air cooled)

The grain size,d, of A2 tool steel sample (heat treated and air cooled) from the peak intensity obtained from the X-ray diffraction :

$$W_{sample}^2 = W_{FWHM}^2 - W_{instr}^2$$

$$W^2 = (1.22)^2 - (0.09)^2$$

$$W = 0.0212\ (0.022\ radians)$$

$$d = \frac{0.9\lambda}{\beta cos\ \theta}$$

$$d = \frac{0.9 * 0.154}{0.0212 * 0.9253} = 7.065nm$$

λ in the equation is characteristic wavelength - $0.154nm$, $0.9253 = \cos\theta = [\ 2\theta = angle\ at\ max.intensity, therefore\ \theta = \frac{angle\ at\ max.intensity}{2}\ ]$

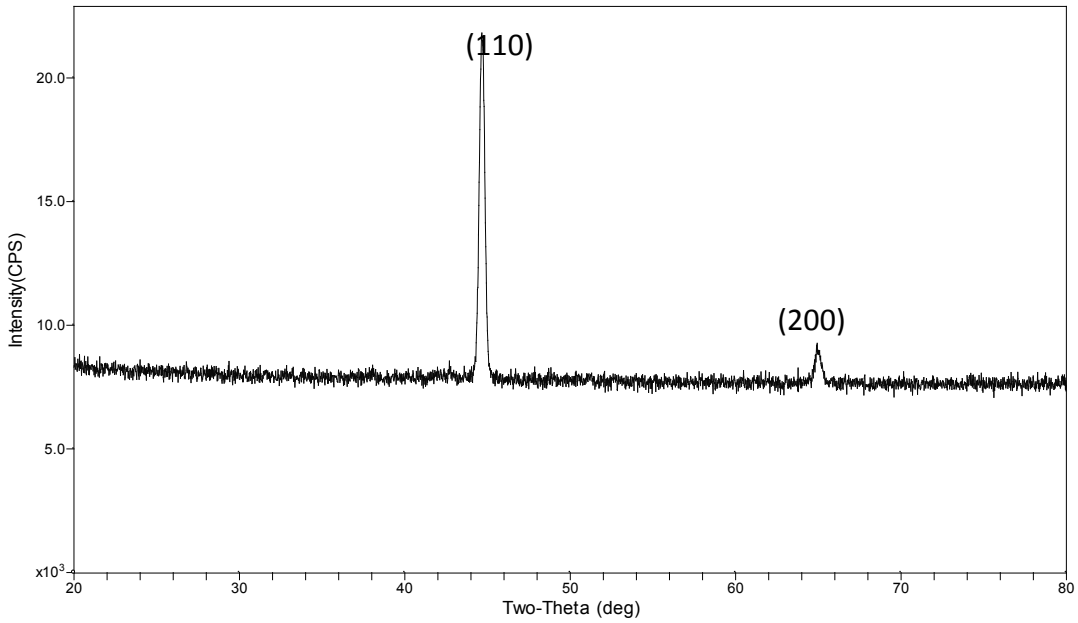

Fig 5.9. XRD pattern for A2 tool steel sample (as received)

The grain size,d of A2 tool steel sample (as received) from the peak intensity obtained from the X-ray diffraction:

$$W_{sample}^2 = W_{FWHM}^2 - W_{instr}^2$$

$$W^2 = (0.57)^2 - (0.09)^2$$

$$W = 0.750\ (0.0131\ radians)$$

$$d = \frac{0.9\lambda}{\beta cos\ \theta}$$

$$d = \frac{0.9 * 0.154}{0.0131 * 0.9253} = 11.438nm$$

λ in the equation is characteristic wavelength - $0.154nm$. $0.9253 = \cos\theta = [\ 2\theta = angle\ at\ max.intensity, therefore\ \theta = \frac{angle\ at\ max.intensity}{2}\ ]$

The XRD results showed that the “heat treated and water quenched” sample of A2 tool steel has the smallest grain size and thus has the highest hardness value.

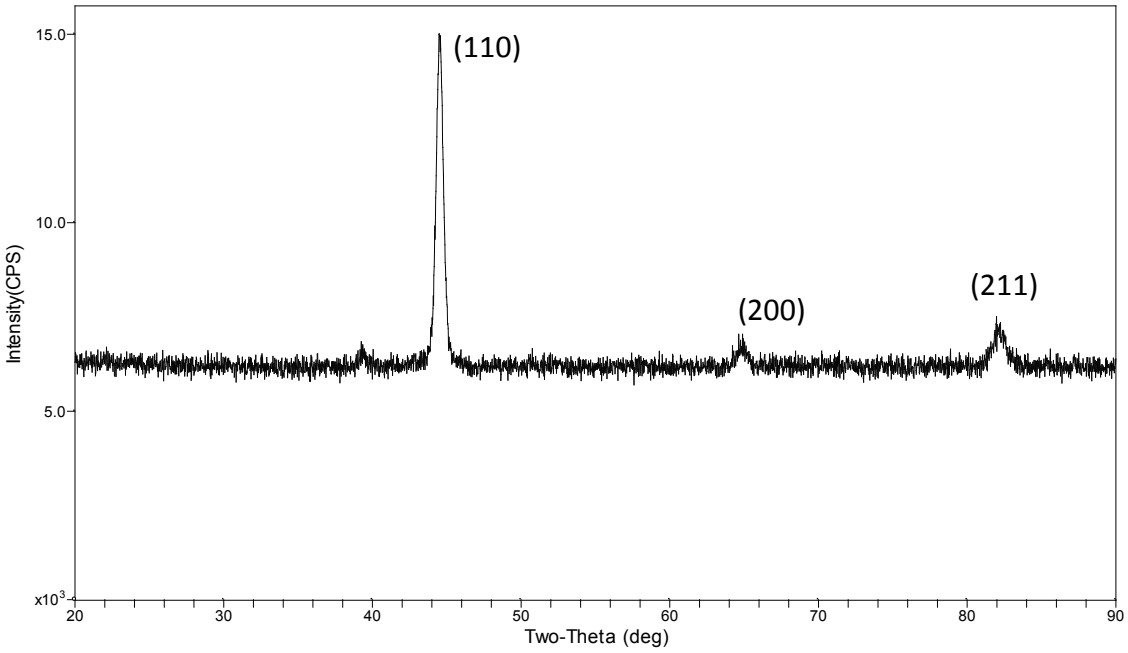

Fig 5.10. XRD pattern for D2 tool steel sample (heat treated and water quenched)

The crystalline grain size, d, of D2 tool steel sample (heat treated and water quenched) from the observed peak intensity of the XRD diffraction is given by:

$$W_{sample}^2 = W_{FWHM}^2 - W_{instr}^2$$

$$W^2 = (0.0172)^2 - (0.09)^2$$

$$W = 0.0147\ (0.01717\ radians)$$

$$d = \frac{0.9\lambda}{\beta cos\ \theta}$$

$$d = \frac{0.9 * 0.154}{0.01717 * 0.9255} = 10.193nm$$

λ in the equation is characteristic wavelength - $0.154nm$, $0.9255 = \cos\theta = [\ 2\theta = angle\ at\ max.intensity, therefore\ \theta = \frac{angle\ at\ max.intensity}{2}\ ]$

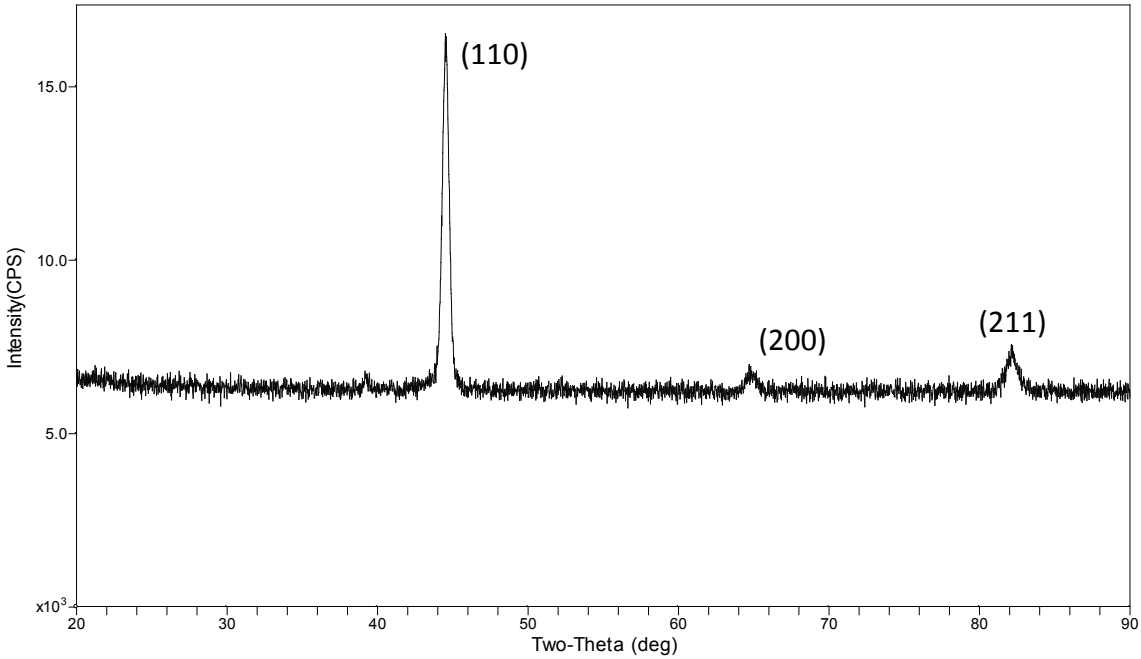

Fig 5.11. XRD pattern for D2 tool steel sample (heat treated and air cooled)

The crystalline grain size, d, of D2 tool steel sample (heat treated and air cooled) from the observed peak intensity of the XRD diffraction is given by:

$$W_{sample}^2 = W_{FWHM}^2 - W_{instr}^2$$

$$W^2 = (0.8)^2 - (0.09)^2$$

$$W = 0.7949 \text{ (0.0138 radians)}$$

$$d = \frac{0.9\lambda}{\beta cos\,\theta}$$

$$d = \frac{0.9 * 0.154}{0.0138 * 0.9255} = 10.851nm$$

λ in the equation is characteristic wavelength - $0.154nm$, $0.9255 = \cos\theta = [\, 2\theta = angle\ at\ max.intensity, therefore\ \theta = \frac{angle\ at\ max.intensity}{2}\,]$

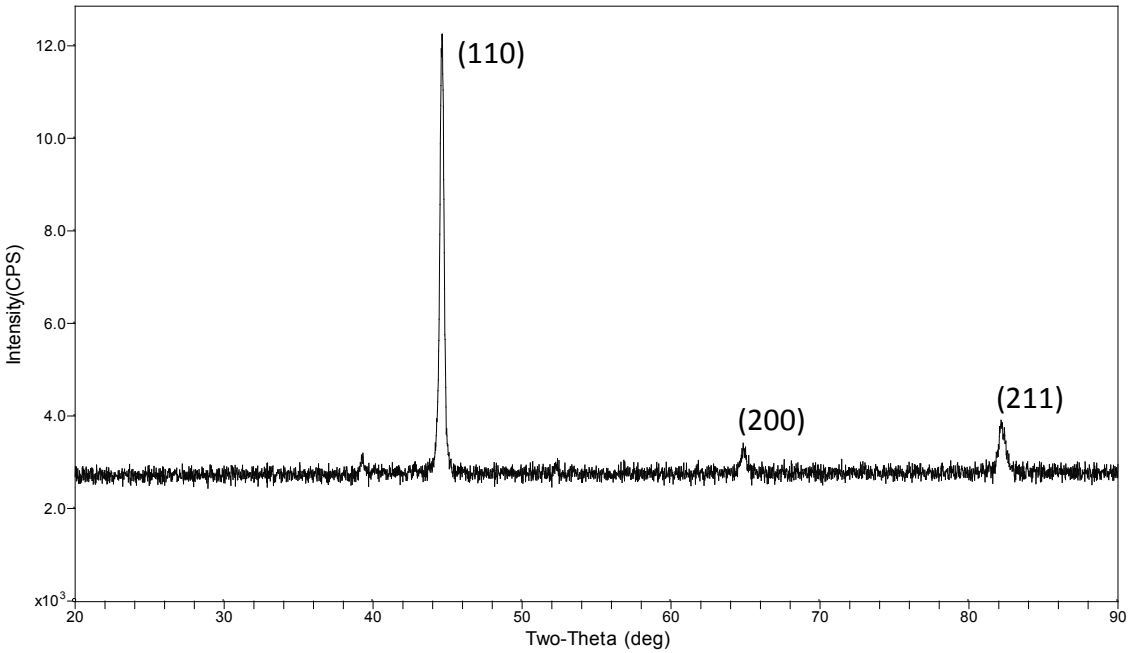

Fig 5.12. XRD pattern for D2 tool steel (as received)

The crystalline grain size, d, of A2 tool steel sample (as received) from the observed peak intensity of the XRD diffraction is given by:

$$W_{sample}^2 = W_{FWHM}^2 - W_{instr}^2$$

$$W^2 = (0.374)^2 - (0.09)^2$$

$$W = 0.363\ (0.022\ radians)$$

$$d = \frac{0.9\lambda}{\beta cos\ \theta}$$

$$d = \frac{0.9 * 0.154}{0.006335 * 0.9255} = 23.653nm$$

λ in the equation is characteristic wavelength - $0.154nm$, $0.9255 = \cos\theta = [\ 2\theta = angle\ at\ max.intensity, therefore\ \theta = \frac{angle\ at\ max.intensity}{2}\ ]$

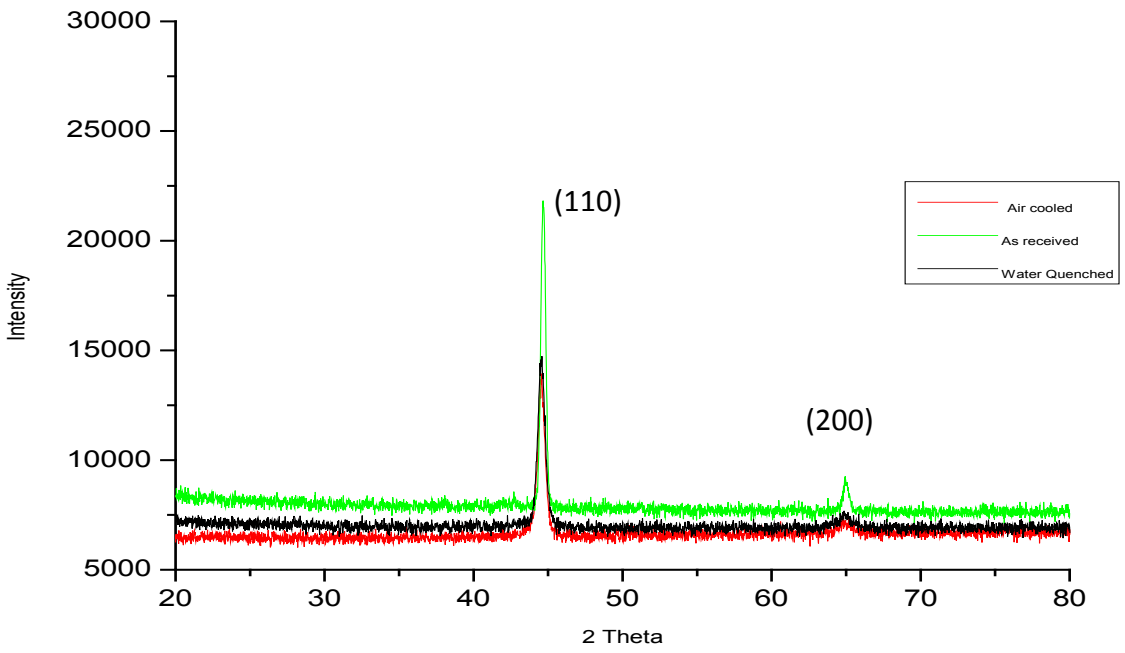

Fig 5.13. Combined XRD pattern for the examined A2 tool steel specimens

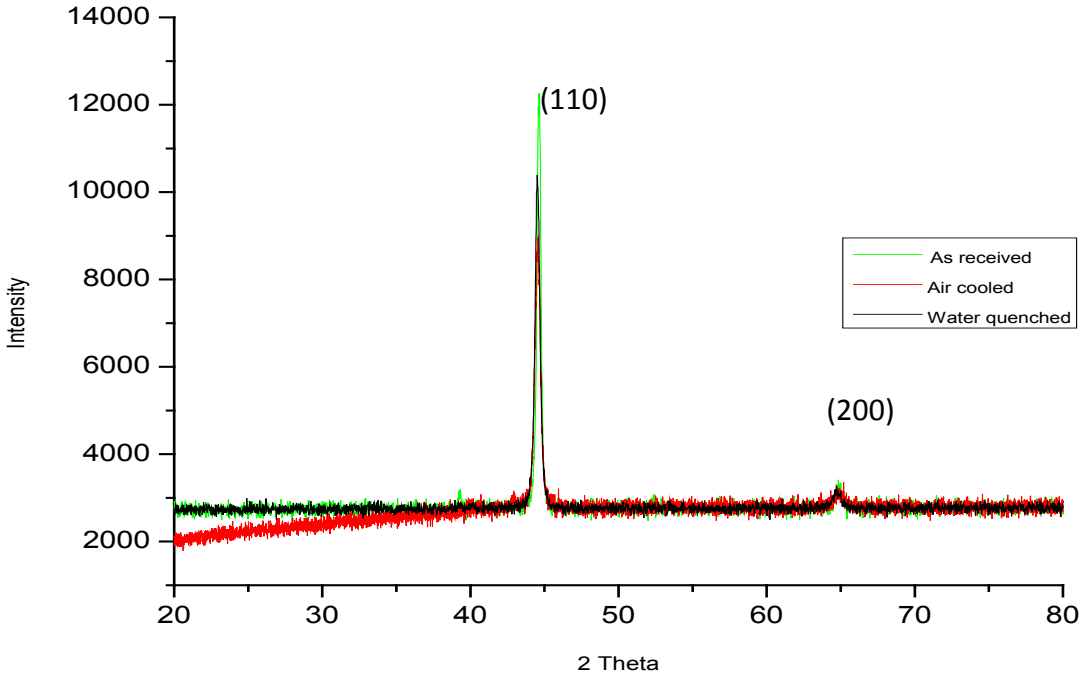

Fig 5.14. Combined XRD pattern for the examined D2 tool steel specimens

Table 5.2: Grain sizes of A2 and D2 tool steel specimens from XRD

Specimen	Grain Size (nm)
A2: As-received	11.44
Heat treated and air cooled	7.07
Heat treated and water quenched	6.81
D2: As received	23.65
Heat treated and air cooled	10.85
Heat treated and water quenched	10.19

The Rockwell C hardness values (Table 5.1) of the all the examined specimens are consistent with the grain size obtained from the XRD results. This shows the correlation of heat treatment on tool steels which correlates well with the changes in the microstructural evolution at austenitizing temperature.

5.4 Nanoindentation

It is important to note that elastic modulus (E) can be thought to be material's resistance to elastic deformation, this property is an intrinsic materials property which can be altered by change in the atomic structure of the material. As can be seen in Fig. 5.12 and 5.13, the elastic modulus values of A2 and D2 tool steels samples approximately remained unchanged in all specimens irrespective of the heat treatment and quenching method used. Hardness (H) on the other hand is not an intrinsic material property because it can be altered by cold-working, heat treatment and other means according to Vlassak and Nix [55] report that modulus (E) is highly dependent on the crystallographic orientation but hardness (H) is not. It might be observed immediately from Fig. 5.14 and 5.15 that the indentation hardness (H)

values for the as-received and the heat treated specimens were clearly distinguishable. The difference observed is indicative of the role different quenching methods play on tool steels hardening process.

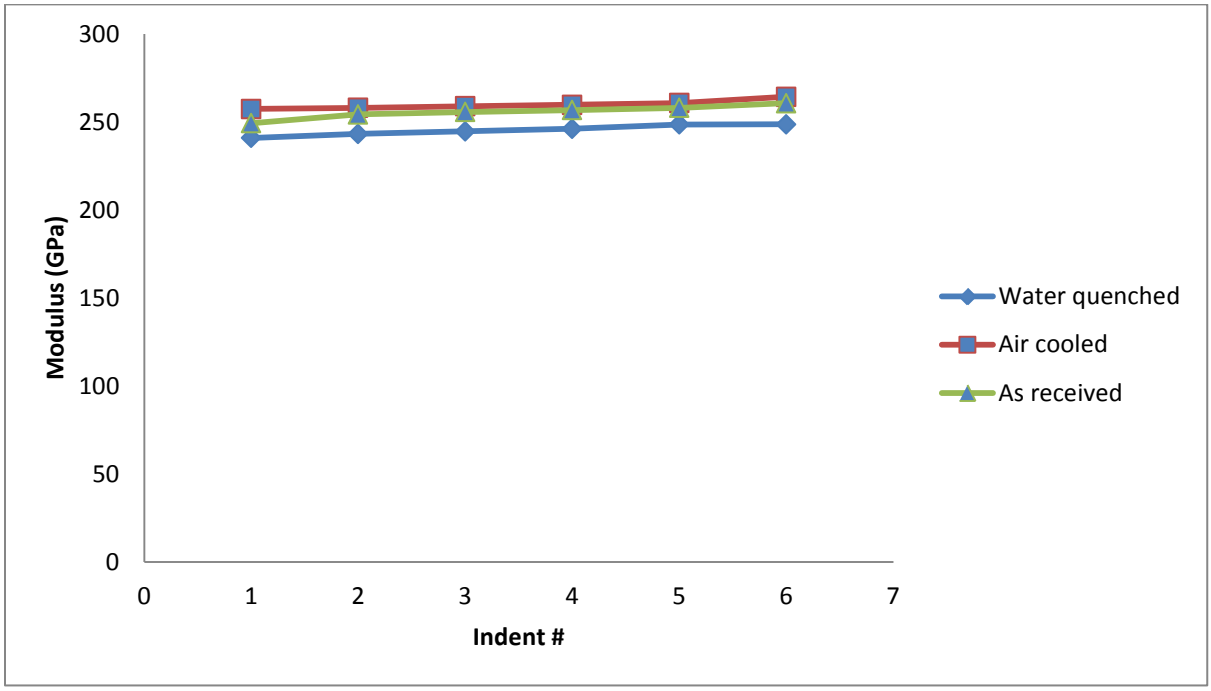

Fig 5.15. Plot of elastic modulus vs. indents at selected locations on D2 tool steel samples

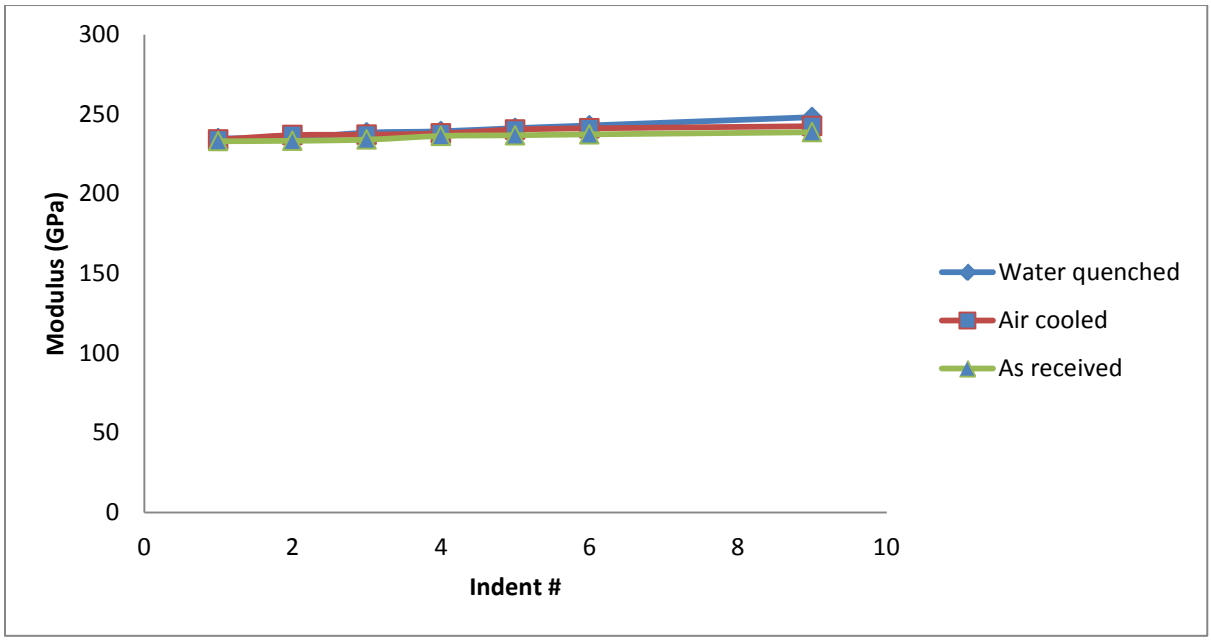

Fig 5.16. Plot of elastic modulus vs. indents at selected locations on A2 tool steel samples

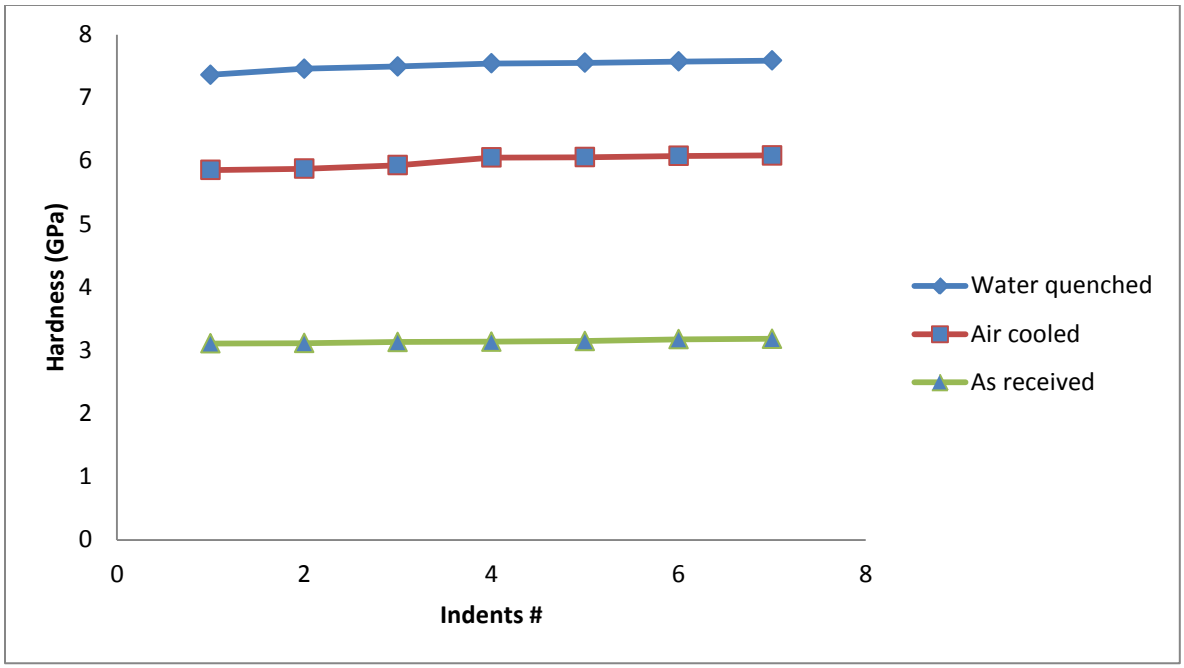

Fig 5.17. Plot of hardness vs. indents at selected locations on D2 tool steels samples

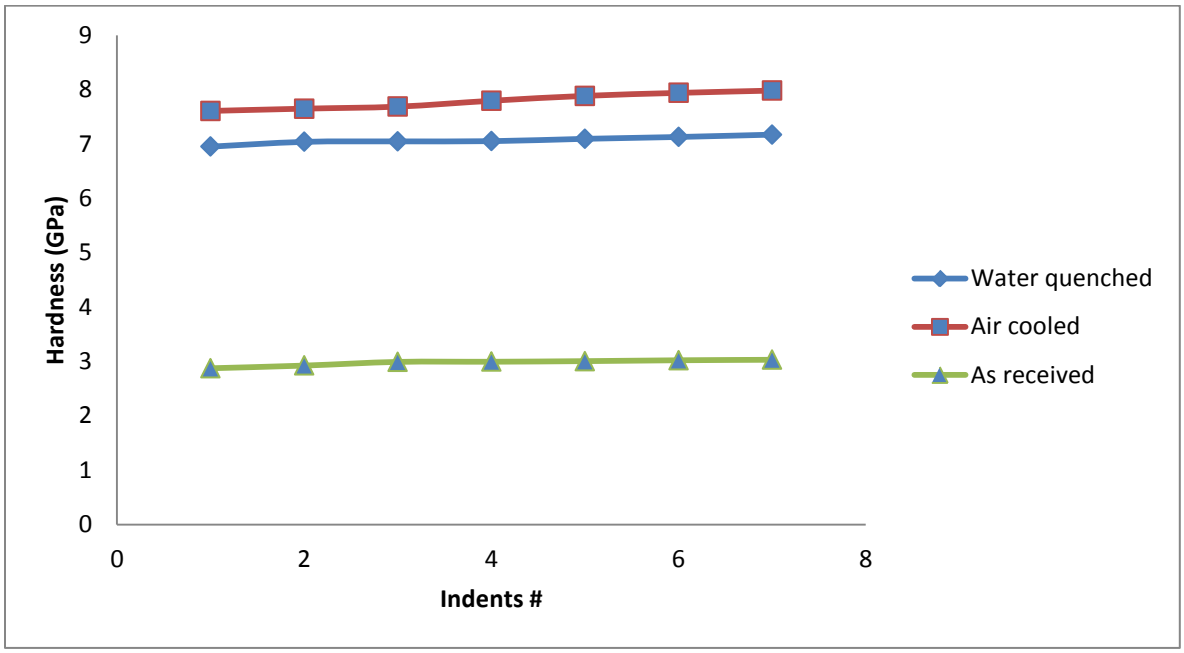

Fig. 5.18. Plot of hardness vs. indents at selected locations on A2 tool steels samples

However, a comparison of the nanoindentation results of A2 tool steel (Fig. 5.15) with the Rockwell hardness result (Table 5.1) showed some unexpected differences; the nanoindentation hardness (H) value for A2 water quenched specimen is lower than that of the

air cool specimen which is not in agreement with the Rockwell hardness result for both specimens. This observed difference could be as a result of the penetration depth at which but both tests were carried out. The Rockwell hardness tester tip penetrated the specimen on a macro scale while nanoindenter tip was at a nano scale. Conversely, the observed increase in hardness (H) value might be attributed to densities of alloy carbide particles present in the material, the Indentation size effect (ISE) [62], the presence of work hardened surface layer [63], surface layers, oxides, chemical contamination, inhomogeneous cooling rate or other factors.

Furthermore, looking at the load-displacement plots, it can be observed quickly that the material recovery rates from the unloading part of the curve of the as-received specimens are much less when compared with the unloading parts of the curve for the heat treated specimens. The observed recovery corresponds to the influence of heat treatment that each specimen has been subjected to thus asserting the brittle nature of the tool steel and hardening process. Again, from the load-displacement curves, one may observe that the load-on-sample for the as-received specimens were much smaller when compared with load-on-sample for the heat treated ones for the same indentation depth; indicative of change in hardness. It can be extracted from the nanoindentation curves that as the indentation hardness value increased the material recovery rate increased also as well as the required load to penetrate the specimen to the desired depth.

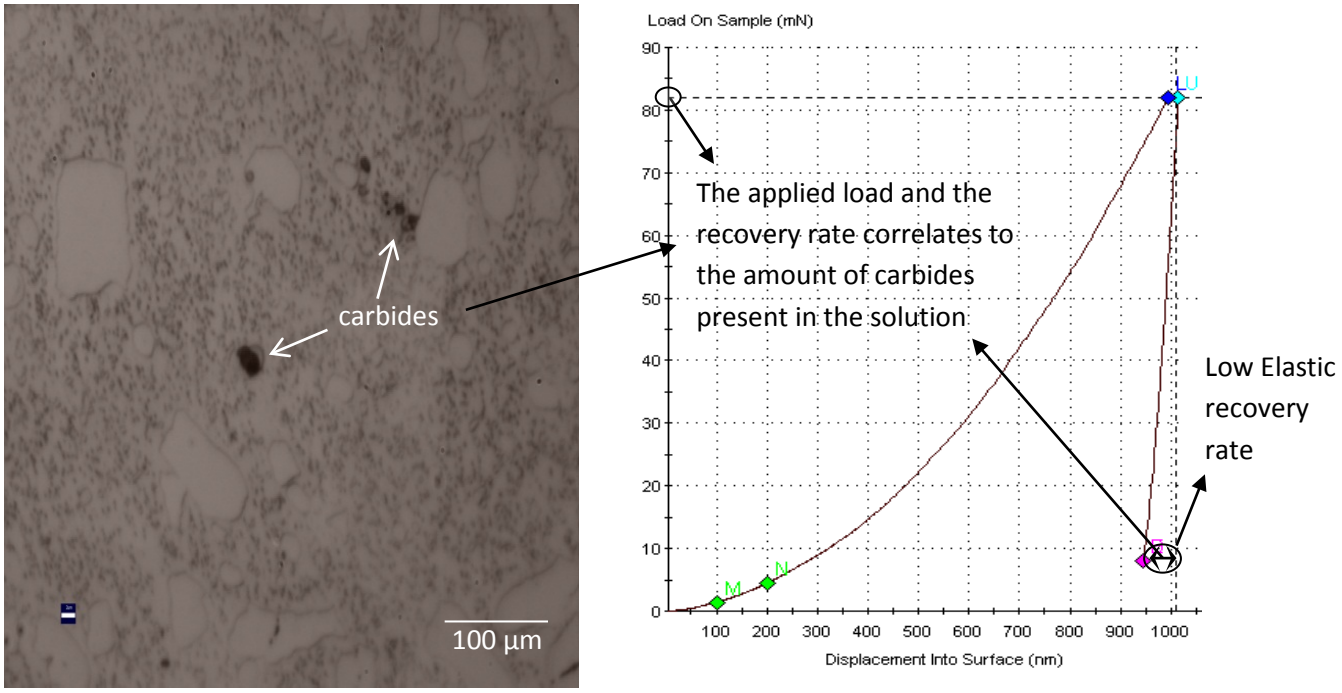

Fig 5.19. Microstructure and load-displacement graph for D2 tool steel sample (as received)

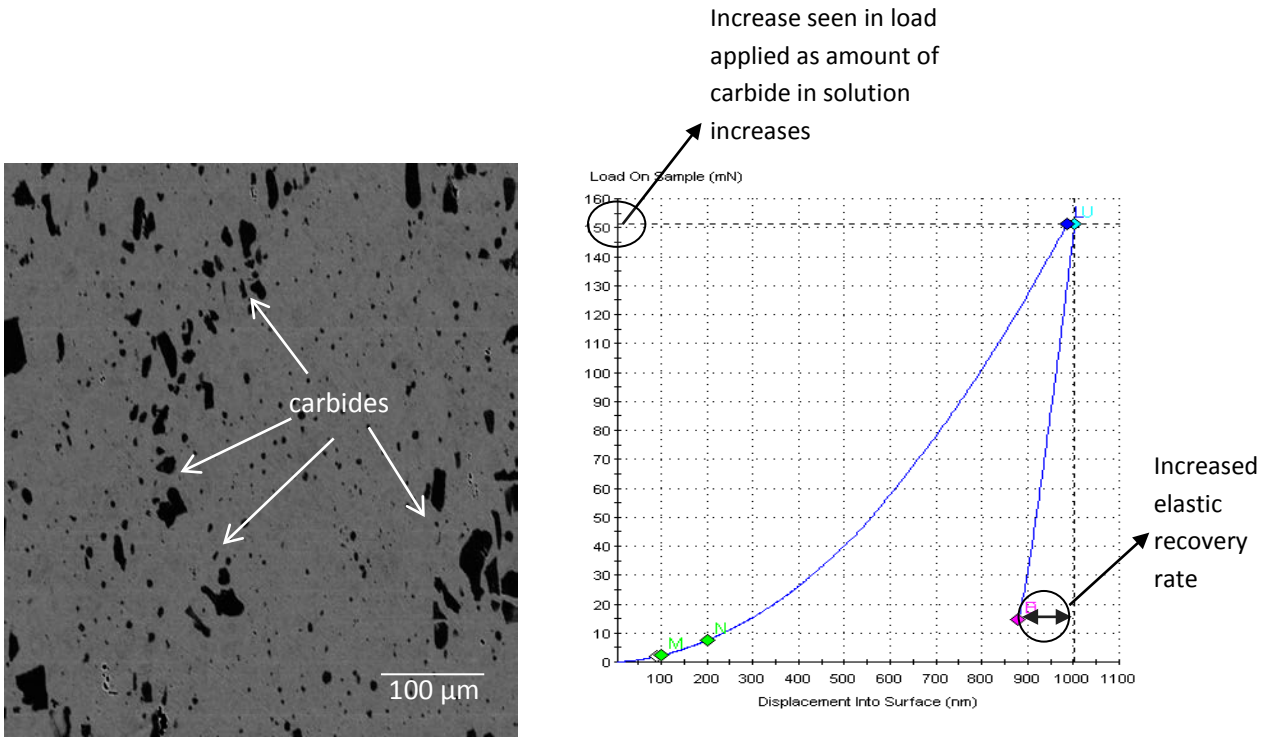

Fig 5.20. Microstructure and load-displacement graph for D2 tool steel sample (heat treated and air cooled)

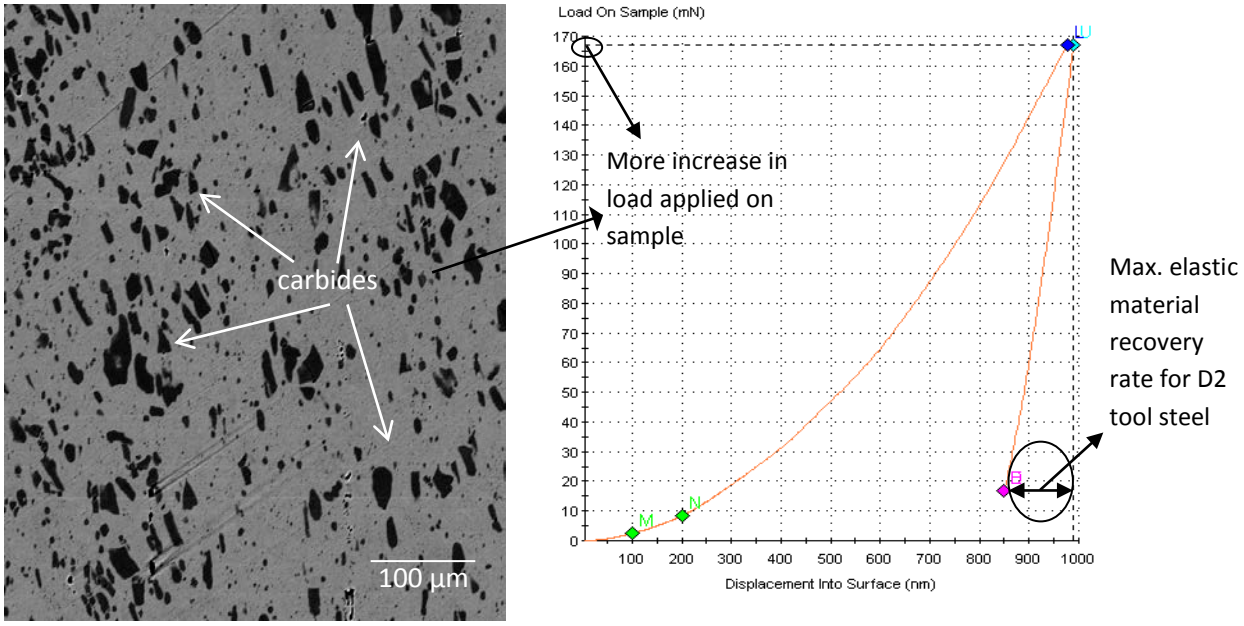

Fig 5.21. Microstructure and load-displacement graph for D2 tool steel sample (heat treated and water quenched)

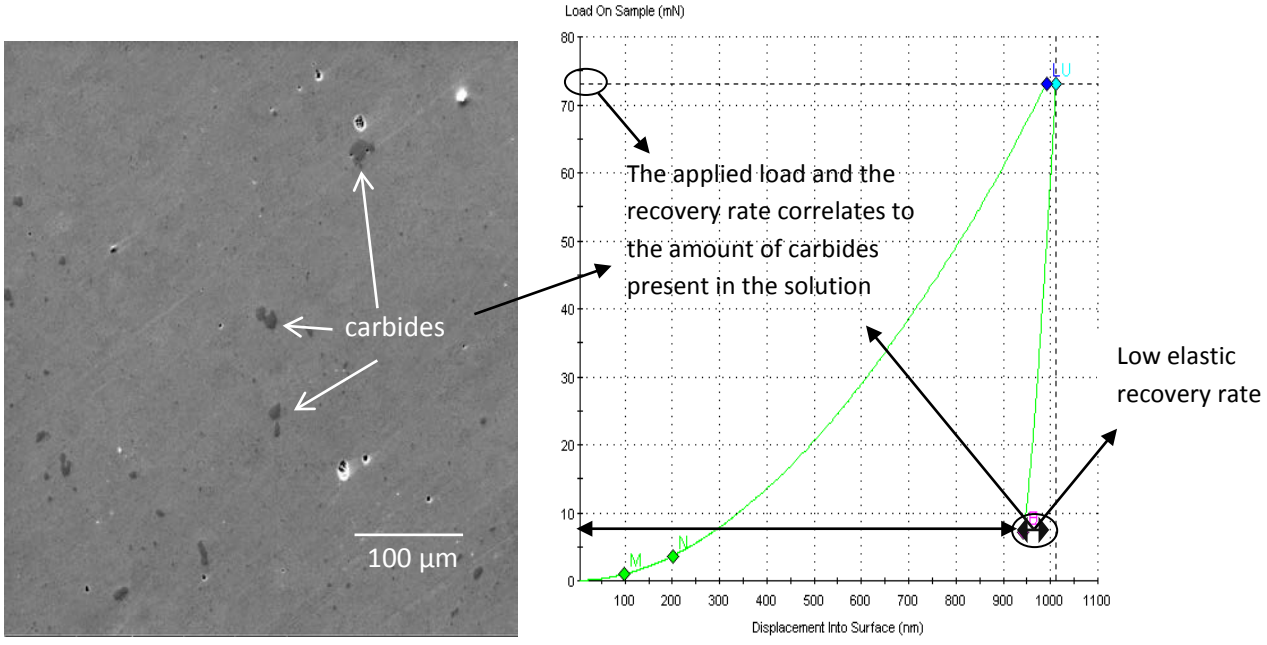

Fig 5.22. Microstructure and load-displacement graph for A2 tool steel sample (As received)

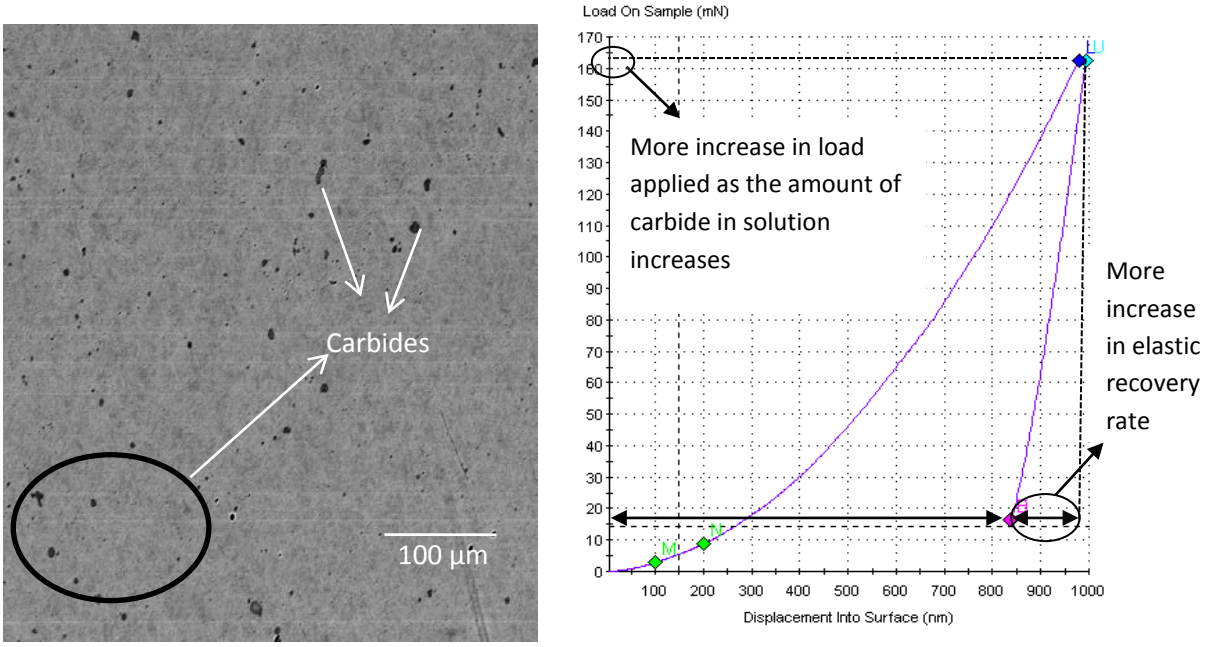

Fig 5.23. Microstructure and load-displacement graph for A2 tool steel sample (heat treated and air cooled)

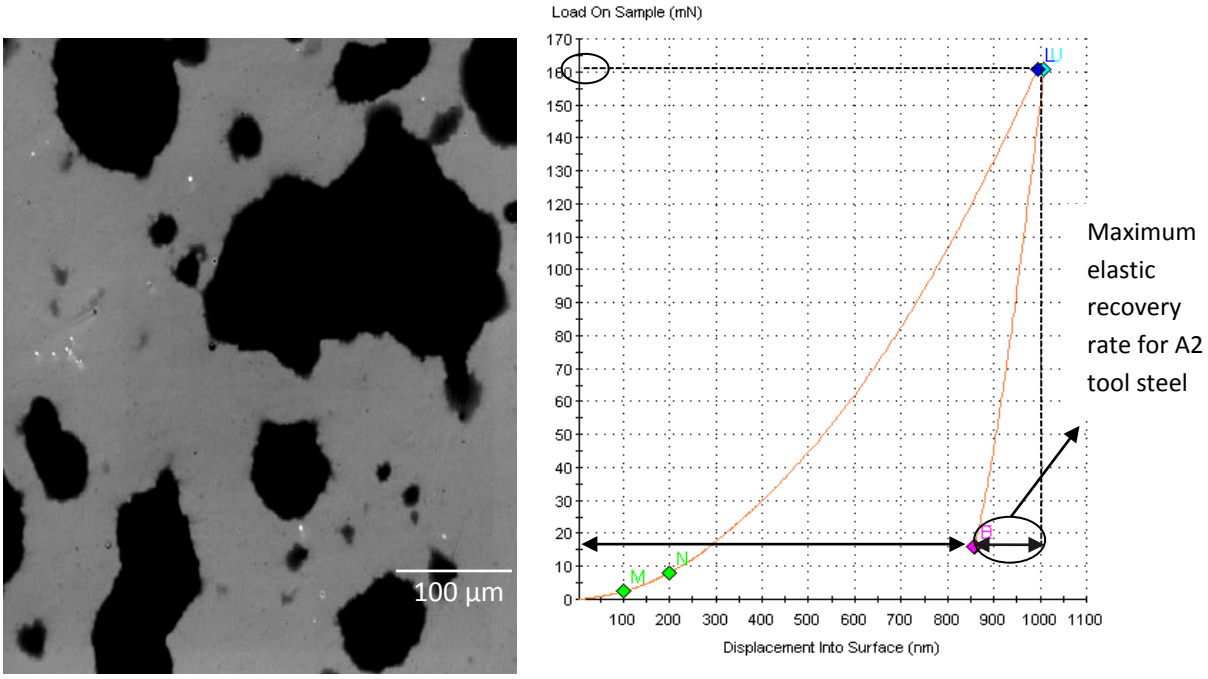

Fig 5.24. Microstructure and load-displacement graph for A2 tool steel sample (heat treated and water quenched)

After series of indentation test on the heat treated samples of A2 and D2 tool steel, no radial crack was observed (Fig. 5.21 and Fig. 5.22). The reason for the absence of radial cracks on the nano scale after indentation is marked for further studies.

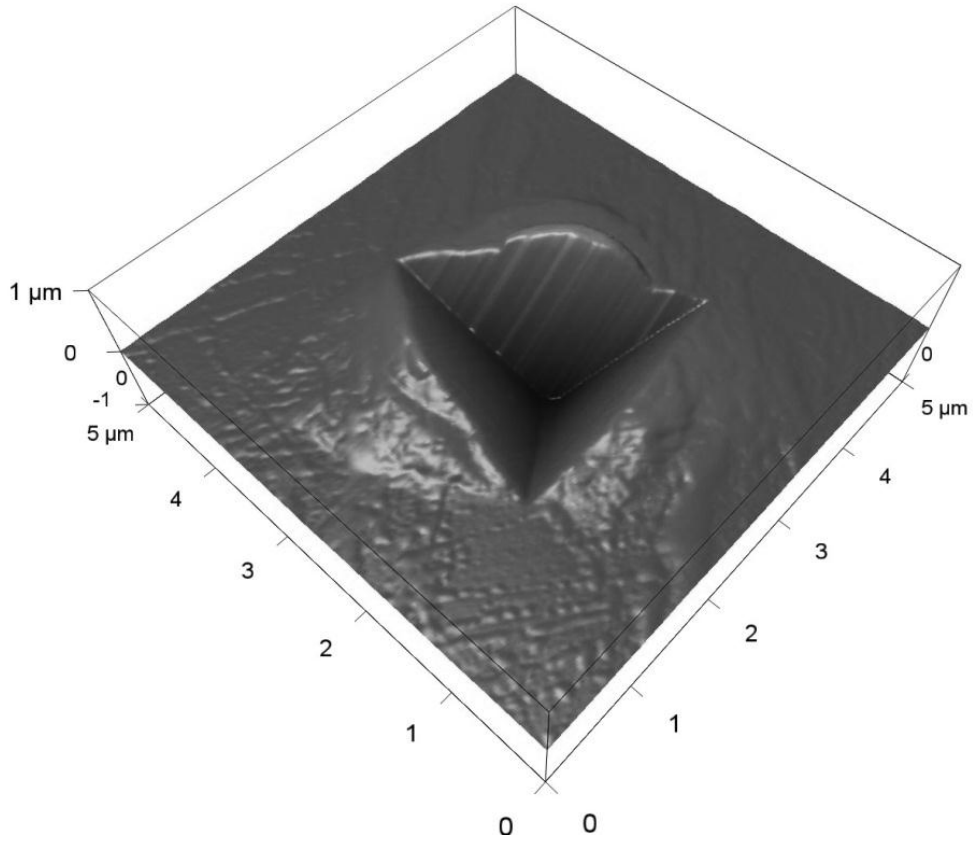

Fig 5.25. AFM image of nanoindentation on a A2 tool steel sample without radial crack

A comparison between the load-displacement graphs for a Berkovich (Fig. 5.27) and a Cube-corner tip (Fig. 5.28) showed a significant increase in the amount of load applied by the indenter on the test material when a Berkovich tip is used during indentation experimentation. This is because the Berkovich indenter has a higher included angle than the Cube-corner indenter.

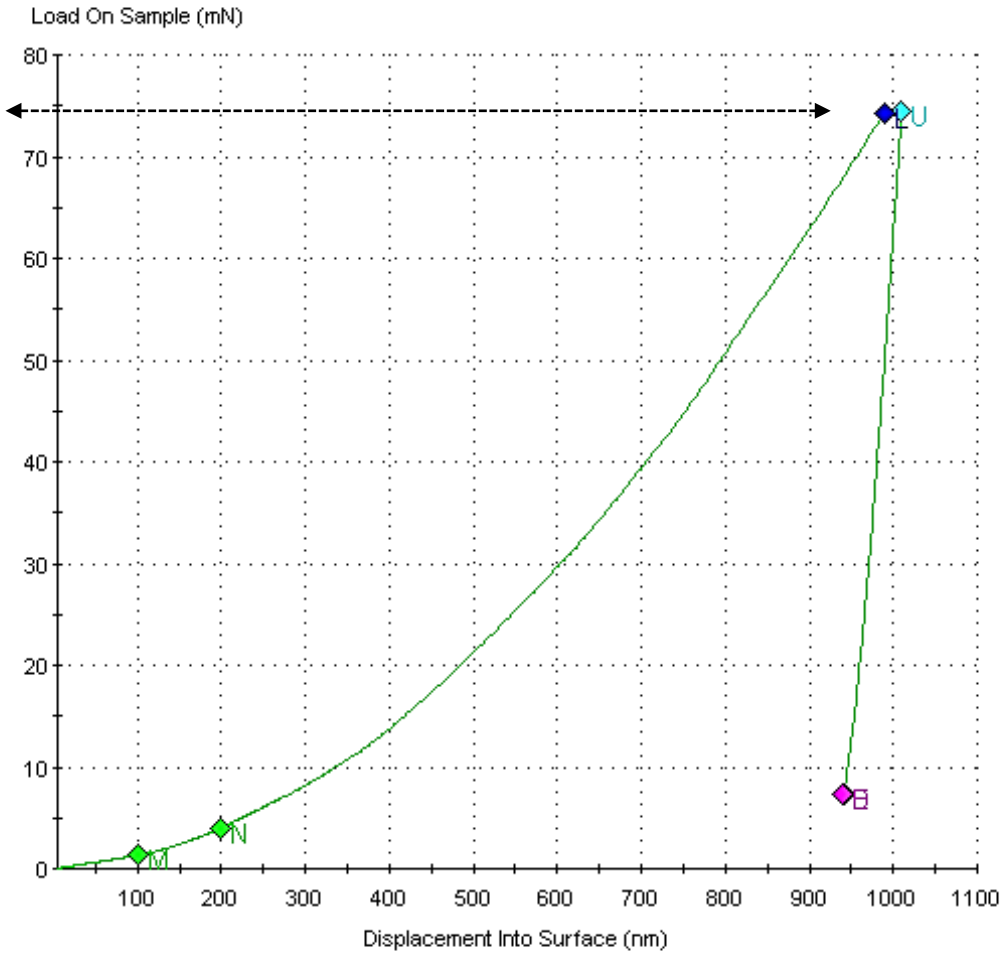

Fig 5.26. Load-displacement graph of A2 tool steel “as received” indented with a Berkovich tip at maximum load of 1000nm.

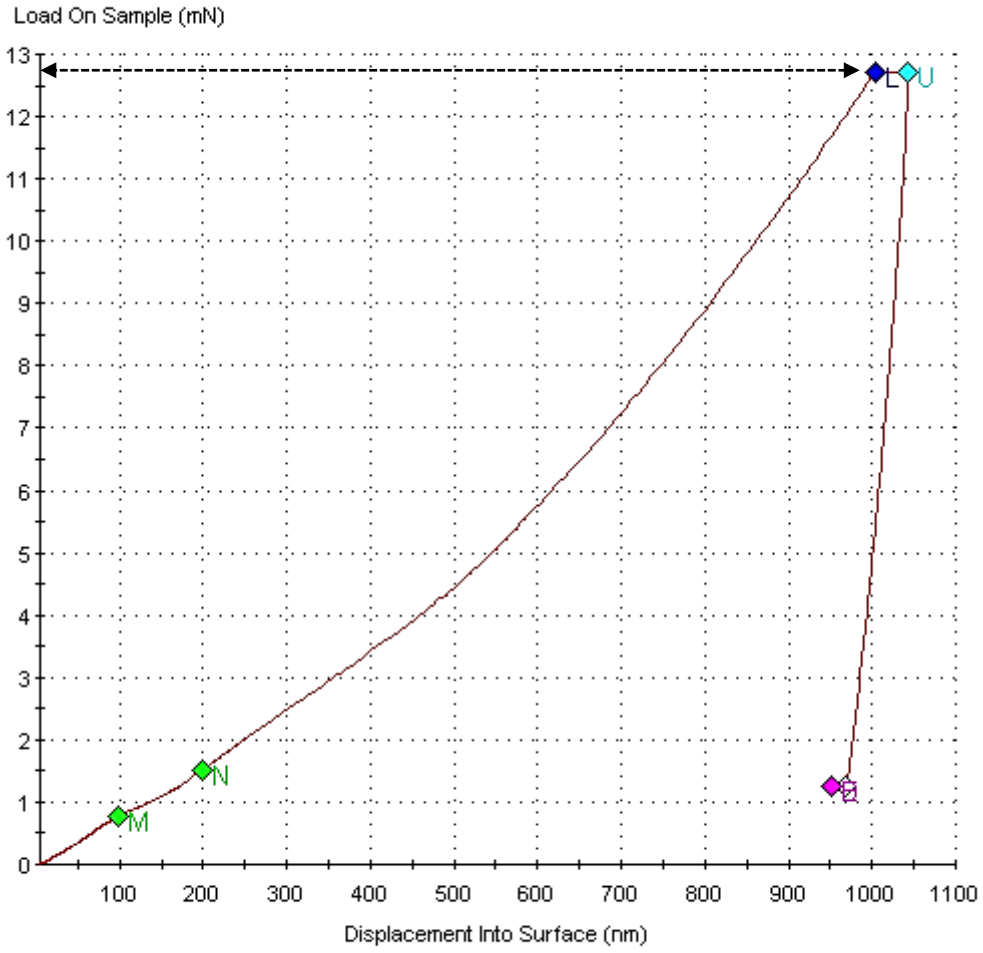

Fig 5.27. Load-displacement graph of A2 tool steel “as received” indented with a Cube corner tip at maximum load of 1000nm.

Changes in indentation hardness were observed as the size of displacement varied in the course of this study. This size dependence which was observed is known as indentation size effect (ISE). For this reason the interpretation of nanohardness measurements is somewhat difficult. Thus, indentation hardness usually cannot be used in modeling or design of brittle products. It is recommended that the hardness be converted to yield strength and research to go beyond the measurement of hardness.

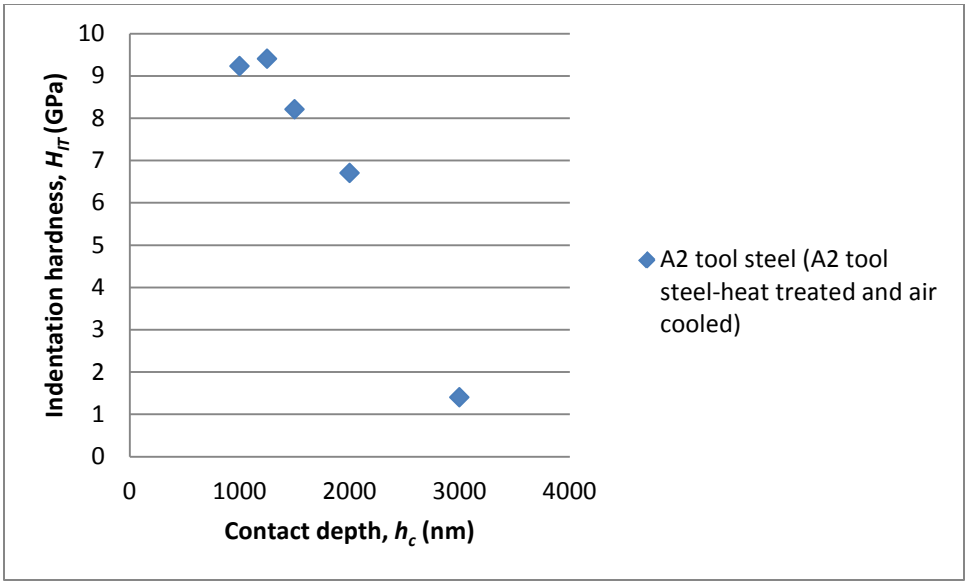

Fig 5.28. Indentation hardness vs. contact depth for A2 tool steel.

The hardness is found to exhibit the size effect i.e., the hardness increases as the indentation depth decreases.

Table 5.3: Avg. hardness and elastic modulus values for A2 tool steel

Type	Load(mN)	Modulus(GPa)	Hardness(GPa)
As received	77	237	2.979
HT* and WQ*	158	234	7.052
HT and AC*	162	238	7.781

HT*= Heat treated, AC*= Air cooled, WQ*= Water quenched

Table 5.4: Avg. of hardness and elastic modulus values for D2 tool steel

Type	Load (mN)	Modulus (GPa)	Hardness (GPa)
As received	80	251	3.491
HT* and WQ*	169	260	7.703
HT and AC*	155	248	6.641

HT*= Heat treated, AC*= Air cooled, WQ*= Water Quenched

5.5 Fracture Toughness of the Silicon Wafer

Increase in indentation depth could not yield any radial crack so the fracture test was marked for further studies on A2 and D2 tool steel. However, a nano indentation on the silicon wafer produced a radical crack which was used to calculate its fracture toughness, K_{IC} according to Lawn equation.

Using Lawn equation: $K_{IC} = \delta \left(\frac{E}{H}\right)^{1/2} \frac{P}{c^{3/2}}$ (19)

where δ, is an empirical constant dependent on the tip, 0.032 for a cube-corner tip, $E\ (GPa)$ is the elastic modulus, $H\ (GPa)$ is the indentation hardness, $P\ (Nm)$ is the maximum indentation load and $c(\mu m)$ is the length of the radial crack on the sample. Equation (19) has been used extensively to determine K_{IC} values in ceramics and hard metals using Berkovich and Vickers indenters in bulk materials without restriction on indentation load [45]. In their work Harding et al [46, 47] found that the cracking threshold can be significantly reduced when an indenter with sharper edges are used. Thus considering the angel between the axis of symmetry and a face for a cube-corner indenter (35.26°) and a Berkovich (65.4°), the rationale for using a cube-corner indenter is quick clear. E and H in equation (19) are determined directly from analyses of the nanoindentation load-displacement data. Indents are made using the cube-corner indenter in an indentation system to generate radial cracks which are measured by imaging the indentation with a nanovision stage.

$$Indenter\ constant, \delta\ =\ 0.032, Young's\ Modulus, E\ (GPa)\ 170.7,\ \ Hardness, H\ (GPa)$$
$$=\ 11.36, P_{\max}(mN) =\ 66.514, Crack\ length, c(\mu m)\ =\ 5.924$$

The calculate fracture toughness for the silicon wafer was $0.5710\sqrt{m}$

This result is close to the reported value range of $0.73\sqrt{m}$-$0.80\sqrt{m}$ [70].

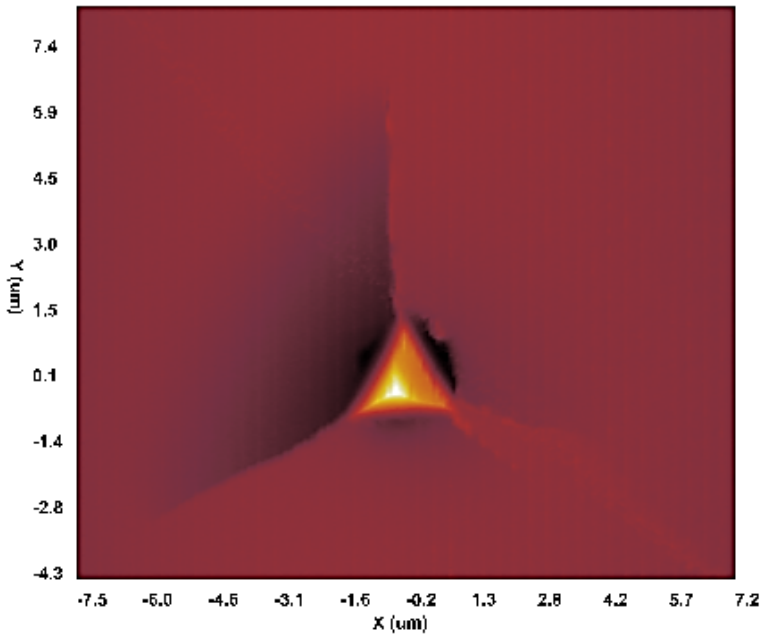

Fig 5.29. Nanovision showing radial cracks from the corner of the cube-corner tip.

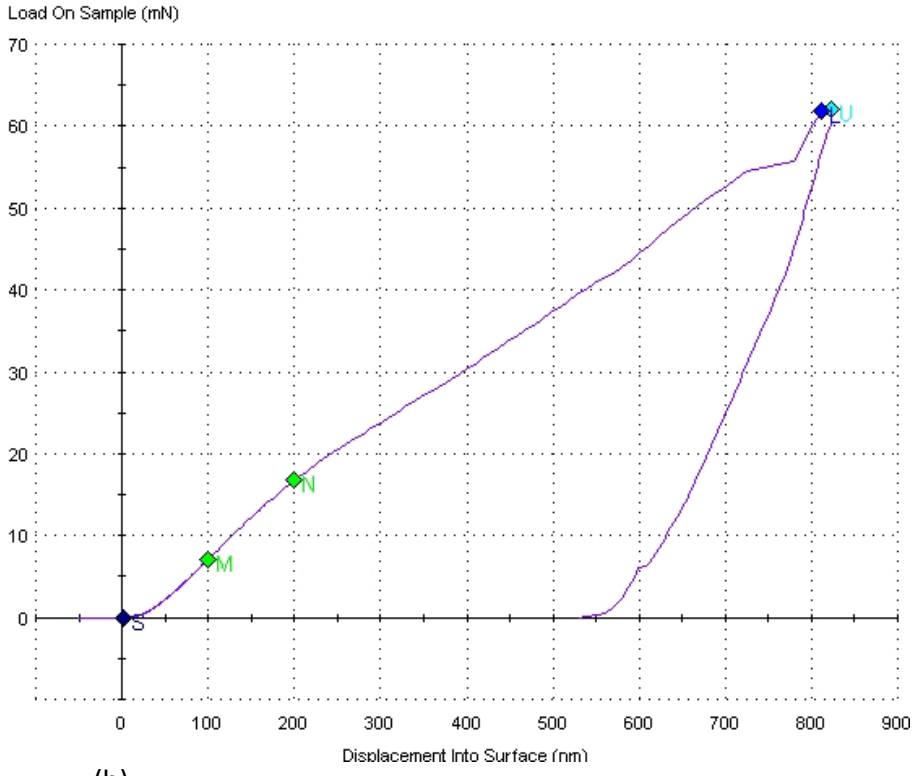

(b)

Fig 5.30. Load-displacement graph of silicon wafer showing “pop-in”on the loading side of the curve.

5.6 Summary

The use of nanoindentation techniques to evaluate the surface mechanical properties of tool steels which cannot be effectively done by conventional means lends support to the importance of this research. Nanoindentation technique has been successfully used to evaluate Hardness (H) and Elastic modulus (E) of A2 and D2 tool steels materials with accuracies of about ± 16% in the absence of pile-up. The use of a cube-corner tip for this research is due to the fact that cube-corner indentation generates stable radial fracture in very small volume. In order words, it significantly reduces the threshold for crack initiation relative to the Vickers and Berkovich tip by more than an order of magnitude. This makes it possible to produce sub-micron indentation with radial cracks in many brittle materials.

The obtained results are useful in the design of surface microstructure that optimize both wear behavior and fracture resistance aimed at developing high-performance tool steels.

Fracture in brittle materials is commonly known as cleavage fracture. It occurs by direct breaking of atomic bonds along the specific crystallographic planes. Cleavage usually involves a low-energy fracture and the surface of the fractures is flat, bright and shiny. Cleavage fracture is mainly seen in BCC, HCP, and ionic and covalently bonded crystals, also in FCC metals that are subjected adverse environment conditions. The “flow “of the “river pattern” seen in cleavage step is believed to be the direction of microscopic crack propagation because the fracture mechanism spreads through grain and grain boundaries. The likelihood of brittleness grows in some material at, higher loading rate and exposure to sever environment.

The research revealed interesting aspects:

(1) Nanoindentation technique proved to be a useful tool in the evaluation of surface hardness, elastic modulus and material ductility in a single test.

(2) Surface hardening effect and indentation depth can affect the indentation hardness results in material characterization.

(3) Further research is proposed / needed to be able to generate radial cracks on hardened A2 and D2 tool steel materials at a nano scale.

(4) The effect of heat treatment and different quenching methods on surface hardness and elastic modulus on the studied materials were examined.

(5) The relationship between heat treatment, material constituent behavior and carbon content of tool steels materials was proved using nanoindentation technique.

(6) The use of nanoindentation experimentation to study the brittleness and ductility of A2 and D2 tool steel materials with respect material constituent behavior showed the extensive application of nanoindentation technique.

REFERENCES

[1] W. Klement, R.H. Willens and P. Duwez, Non-crystalline structure in solidified gold–silicon alloys, Nature. 187 (1960), 869–870.

[2] J.F Shacklefold, Introduction to Material Science for Engineers, pp. 330-331, Macmillian Publishing Company, New York, 1988.

[3] Y.Q. Cheng, E. Ma, Atomic-level structure and structure–property relationship in metallic glasses, Progress in Materials Science. 56 (2011) 379-473.

[4] ISO 12737:2005, Metallic Materials-Determination of Plane-Strain Fracture Toughness.

[5] X. Li, D. Diao, B. Bhushan, Fracture mechanisms of thin amorphous carbon films in nanoindentation, Acta Materialia. 45 (1997) 4453-4461.

[6] P. Chaudhari and D. Turnbull, Structure and properties of metallic glasses, Science. 199 (1978), 11–21.

[7] H.S. Chen, Glassy metals, Rep Prog Phys 43 (1980), 353.

[8] X. Li, D. Diao, B. Bhushan, Fracture mechanisms of thin amorphous carbon films in nanoindentation, Acta Materialia. 45 (1997) 4453-4461 .

[9] M. P blinn and R.A Williams, Design for fracture toughness. Materials characterization laboratory, Volume 20.

[10] A. E. Fischer-Cripps, Nanoindentation Second Edition, pp 27-28, Springer publishing Company, New York, 2004.

[11] G.M. Pharr, Measurement of mechanical properties by ultra-low load indentation, Materials Science and Engineering A. 253 (1998) 151-159.

[12] B.R. Lawn, A.G. Evans and D.B. Marshall. J. Am. Ceram. Soc. 63 (1980), p. 574.

[13] G.R. Anstis, P. Chantikul, B.R. Lawn and D.B. Marshall. J. Am. Ceram. Soc. 64 (1981), 533.

[14] R. Thielsch, K. Kaemmer, B. Holzapfel, L. Schultz, Structure-related optical properties of laser-deposited BaxSr1−xTiO3 thin films grown on MgO (001) substrates, Thin Solid Films. 301 (1997) 203-210.

[15] International perspective on government nanotechnology funding in 2005. Journal of Nanoparticle Research 7 (2005). p. 707-712.

[16] A.P. Ternovskii, V.P. Alekhin, M.Kh. Shorshorov, M.M. Khrushchov, V.N. Skvortsov, Zavod Lab. 39 (1973) 1242.

[17] S.I. Bulychev, V.P. Alekhin, M.Kh. Shorshorov, A.P. Ternovskii, G.D. Shnyrev, Zavod Lab. 41 (1975) 1137.

[18] Love, A.E.H, Philos. Trans. A. 288 (1929) 377.

[19] Love, A.E.H, Quart. J. Math. 10, (1939) 161.

[20] Sneddon, I. N., Int. J. Engng. Sci. 3, (1965) 47.

[21] Harding, J. W., and Sneddon, I. N., Proc. Cambridge Philos. Soc. 41, (1945) 12.

[22] Johnson, K.L., Contact Mechanics, Cambridge University Press, Cambridge, 1985.

[23] Shorshorov, M.Kh., Bulychev, S.I., and Alekhin, V.P. Sov. Phys. Dokl. 26, (1982) 769.

[24] Bulychev, S.I and Alekhin, V.P., Zavod. Lab. 53, (1987) 76.

[25] Olivier, W.C., Hutching, R. and Pethica, J. B., in ASTM STP 889, edited by Blau, P.J. and Lawn, B.R., (American Society of Testing and Materials, Philadelphia, PA 1986), pp. 90-108.

[26] Ternovskii, A.P., Alekhin, V.P., Shorshorov, M.Kh., Khrushchov, M.M., Skvortsov, V.N., Zavod Lab. 39 (1973) p. 1242.

[27] Pharr, G.M., Olivier, W.C., and Brotzen, F. R., J. Mater. Res. 7**,** (1992) 613.

[28] King, R. B., Int. J. Solids Structures 3, (1987) 1657.

[29] Pethica, J.B., in Ion Implantation into Metals, edited by Ashworth, V., Grant, W., and Procter, R., Pergamon Press, Oxford, 1982, pp. 147-156.

[30] W.C. Oliver and G.M. Pharr. *J. Mater. Res.*, 7 (1992), 1564.

[31] Bulychev, S. I., Alekhin, V. P, Shorshorov, M.Kh., Ternovskii, A. P., Prob. Prochn 9 (1976) 79.

[32] W.C. Oliver and G.M. Pharr. *J. Mater. Res.*, 7 (1992), 1564.

[33] Pethica, J.B., Hutchings, R. and Olivier, W.C., Philos. Mag. A. 48, (1983) 593.

[34] R.A Hadfield, Alloys of Iron and chromium, I. iron steel Inst., vol 42 (No. 2) 1898, 40-110).

[35] C.S Smith, A History of metallography and heat treatment, University of Chicago press, 1960.

[36] A. Sauveur, The metallograghic and Heat treatment of iron and steel, McGraw-Hill, 1912; 2nd ed., 1915; 3rd ed., 1926; 4th ed., 1935.

[37] H. Chandler, Ed., Tool steels, Heat treater's Guide: practices and procedures for irons and steels, ASM International, 1995, p. 517-669.

[38] Harding, D.S., Olivier W.C., Pharr, G.M., Mater. Res. Soc. Symp. Proc. 356 (1995) 663.

[39] Manufacturing, Engineering & Technology, Fifth Edition, by Serope Kalpakjian and Steven R. Schmid. ISBN 0-13-148965-8. © 2006 Pearson Education, Inc., Upper Saddle River, NJ.

[40] D.P Koistien and R.E Marburger, Acta Metall., Vol. 7, 1959, p. 59-60.

[41] G. Vander Veort, Deutile and Brittle fractures, metals handbook, 9th ed, vol 11, 2982 p. 85.

[42] R. Hertzberg, Deformation and fracture mechanism of Engineering meterials, 4th ed. John Wiley & sons, Inc., 1996.

[43] C.D Beachem and D.A Meyn: Electron Fractograph, ASTM STP 436, p. 76, ASTM, Philadelphia 1968.

[44] G. Krauss, Heat Treated Martensitic Steels: Microstructural System for Advanced

[45] C.F. Tipper, The Study of Fracture Surface Markings, J. Iron Steel Inst., Vol 185, Jan 1957, p. 4-9.

[46] G.M Boyd, The propagation of fracture in Mild Steel Plates, Engineering, Vol 175, 16 Jan 1953, p 65-69; 23 Jan 1953, p. 100-102.

[47] S. W. Freiman, Brittle Fracture Behavior of Ceramics. *Bull.,* Vol 67 (No. 2), 1998, p. 392.

[48] S.X Wu, Stability and Optimum Geometry of Chevron Notched Three Point Bend Specimens, *Int. J Fract.,* Vol 26 (No. 2), 1984, p. 43-47.

[49] S.W. Freiman, D.R. Mulville, and P.W. Mast S. Nunomura and S. Jitsukawa, Fracture Toughness S853 Evaluation for Bearings Steels by Indentation Cracking under Multi-axial Stress, *Tetsu-to-Haganen,* Vol 64 (No. 5853), 1978 (in Japanese).

[50] Crack Propagation Studies in Brittle Materials, *J. Mater. Sci.,* Vol 8 (No. 11), 1973, p. 1527-1533.

[51] R.M Hemphill and D.E Wert, Impact and Fracture Toughness Testing of Common Grades of Tool Steels, *Tool Materials for molds and dies,* G. Krauss and H. Nordberg, Ed., Colorado School of Mines Press, 1987, p. 66-89.

[52] W.H. Wills, Practical Observatory on High-Carbon High-Chromium Tool Steels, Trans. ASM, Vol 23, 1935, p. 469.

[53] W.H. Wills, Further Study on High-Carbon High Chromium Tool Steels, Trans. ASM, Vol 25, 1937, p. 1013.

[54] J.P Gill, High-Carbon High Chromium Steels, Trans, ASST Vol 15, 1929, p. 367.

[55] Tabor, D. Proc. R. Soc. A 192, (1948) 247.

[56] Stillwell, N.A., and Tabor, D., Proc. Phys. Soc. London 78, (1961) 169.

[57] J.J. Vlassak and W.D. Nix. *J. Mech. Phys. Solids*, 42 (1994), 1223.

[58] Materials Science and Metallurgical, 4th ed., Pollack, Prentice-Hall, 1998.

[59] K.E. Thelning, steel and Its Heat treatment, 2nd ed., Butterworths, 1984.

[60] Introduction to Heat treatment of Tool Steels, Heat treatment, Vol. 4, ASM *Handbook.*

[61] Phillip Agee. Instrumented indentation testing with the Agilent Nano indenter G200, application note.

[62] H. Li, A. Chosh, R.C. Han, Bradt, J. Mater. Res. 8 (1993) 1028.

[63] H. Pelletier, J. Krier, A. Cornet, P. Mille, Thin Solid Films (2000) 147.

[64] Richard A. Krebes (2009) Return To Titanic, By Dr. Robert D. Ballard *Titanic Review* (ref: #9974, accessed 12th March 2012 07:58:04 PM).
URL : http://www.encyclopedia-titanica.org/ballard-return-to-titanic.html

[65] ASM handbooks online Vol. 12, Fractography, Visual examination and light microscopy, interpretation of fractures.

[66] ASM handbook Vol. 11, Failure analysis and prevention, fatigue failures.

[67] G. Bodine, "The Effect of Strain Rate Upon the Morphology of High Purity 26% Chromium, 1% Molybdenum Ferritic Stainless Steel", master's thesis, University of Tennessee 1974.

[68] C.D. Beachem, "Microscopic Fracture Processes" *Fracture,* Vol 1, Academic Press, 1968.

[69] "Fine Ceramics (Advanced Ceramics, Advanced Technical Ceramics)—Test Method for Fracture Toughness of Monolithic Ceramics at Room Temperature by Single Edge Pre-Cracked Beam (SEPB) Method," ISO DIS15732, Geneva, Switzerland, 1999.

[70] D.J Morris and R.F. Cook, “In-Situ Cube-Corner Indentation of Soda-Lime Glass and Fused Silica”, *J. Am Ceram. Soc*., vol 87, no. 8, pp. 1494-1501, 2004.

[71] Micro Star Technologies, Nano indenters from micro star technologies, Revision 2.3, pp. 1.